The antigenic landscape of human influenza N2 neuraminidases from 2009 until 2017

João Paulo Portela Catani[1,2], Anouk Smet[1,2], Tine Ysenbaert[1,2], Marnik Vuylsteke[3], Guy Bottu[4], Janick Mathys[4], Alexander Botzki[4], Guadalupe Cortes-Garcia[5], Tod Strugnell[5], Raul Gomila[5], John Hamberger[5], John Catalan[5], Irina V. Ustyugova[5], Timothy Farrell[5], Svetlana Stegalkina[5], Satyajit Ray[5], Lauren LaRue[5], Xavier Saelens[1,2*], Thorsten U. Vogel[5*]

[1]VIB Center for Medical Biotechnology, VIB, B-9052 Ghent, Belgium

[2]Department of Biochemistry and Microbiology, Ghent University, B-9052 Ghent, Belgium

[3]Gnomixx, Melle, Belgium

[4]VIB Bioinformatics Core, VIB, B-9052 Ghent, Belgium

[5]Sanofi, Research North America, Cambridge, Massachusetts, USA

* Corresponding authors:

E-mail: Xavier.saelens@vib-ugent.be and Thorsten.Vogel@sanofi.com

Abstract

Human H3N2 influenza viruses are subject to rapid antigenic evolution which translates into frequent updates of the composition of seasonal influenza vaccines. Despite these updates, the effectiveness of influenza vaccines against H3N2-associated disease is suboptimal. Seasonal influenza vaccines primarily induce hemagglutinin-specific antibody responses. However, antibodies directed against influenza neuraminidase (NA) also contribute to protection. Here, we analyzed the antigenic diversity of a panel of N2 NAs derived from human H3N2 viruses that circulated between 2009 and 2017. The antigenic breadth of these NAs was determined based on the NA inhibition (NAI) of a broad panel of ferret and mouse immune sera that were raised by infection and recombinant N2 NA immunization. This assessment allowed us to distinguish at least 4 antigenic groups in the N2 NAs derived from human H3N2 viruses that circulated between 2009 and 2017. Computational analysis further revealed that the amino acid residues in N2 NA that have a major impact on susceptibility to NAI by immune sera are in proximity of the catalytic site. Finally, a machine learning method was developed that allowed to accurately predict the impact of mutations that are present in our N2 NA panel on NAI. These findings have important implications for the renewed interest to develop improved influenza vaccines based on the inclusion of a protective NA antigen formulation.

43 **Introduction**

44 Neuraminidase (NA) and hemagglutinin (HA) constitute the two major antigenic proteins at the
45 surface of influenza A and B virions (Uyeki et al., 2022). While HA mediates binding to sialic acids and
46 membrane fusion, NA catalyses the removal of sialic acid residues from sialylated glycoproteins and
47 glycolipids. This complementary role of HA and NA enables influenza virions to penetrate the mucus
48 barrier that lines the respiratory epithelium and newly formed virions to be released from the
49 infected cell (de Vries et al., 2020; Matrosovich et al., 2004; Palese et al., 1974). Immunity against
50 influenza is associated with the presence of anti-HA antibodies in serum, as determined by a
51 hemagglutination inhibition assay. In line with this, the composition of licensed influenza vaccines is
52 primarily focused on the antigenic characteristics of HA as the protective vaccine antigen (Cox,
53 2013). Multiple studies, however, have underscored the protective potential of anti-NA immune
54 responses as determined by NA inhibition (NAI) assays (Couch et al., 2013; Maier et al., 2019;
55 Memoli et al., 2016; Monto and Kendal, 1973; Monto et al., 2015; Ng et al., 2019; Weiss et al., 2019).
56 There is also evidence that pre-existing anti-N2 immunity induced by prior exposure to H2N2 viruses
57 that circulated in the population from 1957 to 1968, tempered the impact of the H3N2 pandemic
58 virus that emerged in 1968 (Eickhoff and Meiklejohn, 1969; Jester et al., 2020; Monto and Kendal,
59 1973; Viboud et al., 2005). Further, the pharmacological inhibition of NA activity is a well-established
60 therapeutic strategy to try to reduce influenza severity and duration (Leneva et al., 2000; Yen et al.,
61 2005). In addition, antibodies with NAI activity can protect against influenza virus infection in pre-
62 clinical models (Chen et al., 2018; Deroo et al., 1996; Rosu et al., 2022; Wan et al., 2018; Wohlbold et
63 al., 2017).

64 Since its appearance in 1968, human H3N2 viruses have been evolving faster than the co-circulating
65 H1N1 and influenza B viruses (Bedford et al., 2014; Potter et al., 2019). The overall Influenza virus
66 vaccine effectiveness varies between seasons and, despite frequent updates of the H3N2 HA
67 component, the effectiveness of influenza vaccines against H3N2-associated disease ranges between
68 5 and 39%, which is lower than the effectiveness against H1N1 and influenza B (Belongia et al.,
69 2016). In this context the use of NA as a complementary vaccine antigen might improve influenza
70 vaccine effectiveness, for example by compensating for HA-based antigenic mismatches in
71 circulating influenza virus strains (Krammer et al., 2018).

72 Phylogenetic analyses of HA and NA genes of human H3N2 viruses revealed the asynchronous
73 evolution of the 2 proteins. In addition, the evolutionary rate as determined by the accumulation of
74 mutations over time, is estimated to be 1.5 times lower for NA than for HA (Westgeest et al., 2012).
75 Despite the strong evidence that immune responses directed against NA can contribute to

76 protection against influenza, a comprehensive insight in the antigenic breadth and evolution of the
77 H3N2 NA antigen is lacking (Nachbagauer et al., 2017; Rajendran et al., 2017; Smith et al., 2004;
78 Westgeest et al., 2012).

79 Here, we determined the antigenic landscape of N2 NAs derived from human H3N2 strains that were
80 isolated between 2009 and 2017. This analysis allowed the identification of at least 4 N2 NA
81 antigenic groups and to estimate the weight of amino acid changes on their contribution to NA
82 antigenic drift.

83 **Results**

84 **Generation of H3N2-derived NA immune sera in ferrets and mice**

85 Our aim was to determine the antigenic relationship between NAs derived from human H3N2
86 viruses that circulated during nearly one decade. We first selected 44 H3N2 neuraminidase protein
87 sequences obtained via GISAID, derived from viruses that were isolated between 2009 and 2017
88 (Elbe and Buckland-Merrett, 2017). Hierarchical clustering with minimax linkage was employed to
89 ensure the set was representative of overall protein sequence diversity (Bien and Tibshirani, 2011).
90 Next, 44 recombinant H1N2 viruses were generated that carried the internal and HA genes from PR8
91 virus and the NA genes of the selected H3N2 viruses. In addition, the corresponding tetrabrachion-
92 stabilized recombinant N2 NA proteins were produced in Chinese hamster ovary (CHO) cells and
93 purified, and are referred to as NACHOs (Catani et al., 2022). All purified NACHOs were tetrameric
94 based on SEC-MALS analysis. The enzymatic activity of the NACHOs was determined based on the
95 hydrolysis of the fluorogenic small molecule substrate 4-methylumbelliferyl-N-acetylneuraminic acid
96 (MUNANA). The NACHOs were active with a specific activity ranging from 0.27 to 27.48
97 nmole/min/µg, indicating correct folding and assembly of the NA head domains (Table S1).

98 Immune sera against all 44 H3N2-derived NAs were generated in pairs of ferrets by a primary
99 infection with the respective H1N2 reassortant viruses. This prime by infection was used to avoid the
100 use of an adjuvant upon subsequent boost with the corresponding NACHOs. On day 28 after primary
101 infection, all animals were boosted by intramuscular injection of homologous NACHO, except for the
102 ferrets that had been primed by infection with A/Stockholm/15/2014 and A/Estonia/91621/2015,
103 which were re-inoculated with the same respective H1N2 reassortant viruses. These two pairs of
104 ferrets were not boosted with homologous NACHO because the corresponding NACHOs were not
105 available at the time of the experiment. Blood samples were taken from the ferrets on days 14 and
106 42 after (primary) infection (Figure 1a). Priming by H1N2 infection resulted in seroconversion against
107 the respective immobilized homologous NACHOs (Figure 1b). Subsequent immunization with

108 recombinant NACHOs boosted the NACHO-specific IgG titers in day 42 serum samples. In contrast,
109 serum samples from the ferrets that had been re-inoculated with H1N2 reassortant carrying NA
110 derived from A/Stockholm/15/2014 or A/Estonia/91621/2015, showed no further increase in titers,
111 presumably because prior exposure with the same H1N2 virus had induced a sterilizing immune
112 response (Figure 1b).

113 We also generated NA immune sera in BALB/c mice. Groups of 5 mice were immunized two times,
114 with a two-week interval, by intramuscular injection with 1 µg of the respective 43 NACHOs
115 adjuvanted with AF03 (the NACHO A/West-Virginia/17/2012 was not available for mice
116 immunization and ELISAs). Blood was collected from the immunized mice and serum prepared on
117 day 28 after the prime immunization (Figure 1c). NACHO-specific IgG titers in the mouse immune
118 sera, pooled from each group, ranged from 1:8100 to 1:72900 (Figure 1d).

119 **The antigenic profile of N2 neuraminidase**

120 Next, NAI titers were determined in the ferret sera using a panel of H6N2 reassortant viruses in an
121 enzyme-linked lectin assay (ELLA), avoiding interference by anti-H1 HA antibodies in this assay. We
122 generated 27 H6N2 influenza viruses with H6 HA derived from A/mallard/Sweden/2002 and NA
123 derived from a subset of the 44 H3N2 viruses, thereby retaining NA sequence diversity and year of
124 H3N2 virus isolation (Table S2). The 27 H6N2 viruses could be classified into 4 groups when ordered
125 according to the phylogenetic relatedness of their NA sequence (Figure 2). The conversion rate of
126 MUNANA into 4-methylumbelliferyl and acetylneuraminic acid by these H6N2 viruses revealed a K_M
127 that ranged from 20.7 to 144.8 µM as determined by the Michaelis-Menten equation (Figure 2 –
128 figure supplement 1a and table S2). Interestingly, the K_M differs between the distinct phylogenetic
129 groups (Figure 2 – figure supplement 1a). There was a negative correlation between the K_M values
130 and the dilution of the H6N2 viruses required to set the 70% maximal NA activity in ELLA (Figure 2 –
131 figure supplement 1b and table S2).

132 Using this panel of 27 H6N2s, we determined the NAI titers in the sera obtained from the 44 pairs of
133 ferrets 2 weeks after the boost. ELLAs were performed in duplicate for all serum samples against one
134 H6N2 target at the same time. The reciprocal NAI titers of the ferret sera paired with H6N2 viruses
135 are shown in table S3. In general, the NAI titers of the ferret sera were the highest against
136 homologous and phylogenetically closely related H6N2 viruses.

137 In Figure 2, all the tested ferret sera are represented in the rows and the 27 H6N2 viruses against
138 which the sera were evaluated in ELLA are presented in the columns. The serum samples were
139 ordered according to the phylogenetic relatedness of the N2 NA head domain amino acid sequences,

140 showing that these cluster in 4 groups (G1-G4). The ELLA-based IC_{50} NAI titers were plotted relative
141 to the maximum NAI titer obtained against the respective H6N2 target viruses. The heatmap thus
142 represents, for each H6N2 virus, the normalized ELLA IC_{50} titer expressed as log_2 of the fold-
143 difference relative to the serum with the highest IC_{50} value against that H6N2 virus (dark red squares
144 indicate high and blue squares low IC_{50} values) (Figure 2).

145 Next, these normalized NAI values were clustered against each of the H6N2s using the Unweighted
146 Pair Group Method with Arithmetic Mean (UPGMA), which is a distance-based method. This
147 clustering allowed to discern at least 4 major antigenic clusters (AC1 to -4) that are depicted at the
148 top of the heat map (Figure 2). It is interesting to note that the H6N2 viruses with NA antigens
149 derived from A/Wisconsin/16/15, A/Alaska/251/15, and A/Kansas/14/2017 do not segregate into
150 AC2, as would be predicted based on the phylogenetic relatedness, but cluster in AC1 based on the
151 UPGMA. However, the overall concordance of the antigenicity with the phylogenetic relatedness,
152 based on the amino acid sequences of the NA head domains, was confirmed by hierarchical
153 clustering with bootstrapping and k-means (Figure 2 – figure supplements 2a and 2b). In line with
154 this, a positive correlation was observed between the pairwise phylogenetic distances and the
155 normalized NAI IC_{50} values for each of the tested H6N2s (Figure 2 – figure supplement 3).

156 We further tested the NAI activity of ferrets' sera obtained 2 weeks after the prime infection against
157 at least one H6N2 virus from each antigenic cluster. These H6N2 viruses were selected based on
158 their antigenic relatedness as deduced from the ferret immune sera analysis (Figure 2) with 2
159 representatives from group 1 (Tex12, and Per09) and 1 each from group 2 (Kan17), group 3 (Hel823),
160 and group 4 (Ind11). The normalized data confirmed the antigenic clustering observed in sera after
161 boost (Figure 2 – figure supplement 4).

162 The NAI titers were also determined in the sera obtained from the 43 groups of NACHO-immunized
163 mice against 7 of the H6N2 viruses. These H6N2 viruses were selected as described above with the
164 addition of HK14 and Swi13 H6N2s, both belonging to antigenic cluster 1. Serum NAI IC_{50} values
165 against a given H6N2 virus were normalized against the IC_{50} of the mouse serum that had the highest
166 NAI titers against the tested H6N2 virus. UPGMA-based clustering showed that the mouse NACHO
167 immune sera displayed a similar recognition pattern as the ferret immune sera that had been
168 generated by H1N2 priming followed by a NACHO boost (Figure 2). For example, HK14 H6N2 NA
169 activity is strongly inhibited by sera from group 1, is poorly inhibited by most of the sera from group
170 2 and is hardly inhibited by group 3 and 4 sera from both ferrets and mice. Ind11 H6N2 NA activity,
171 on the other hand, was inhibited by group 1 and 4, and hardly by group 2 and 3 immune sera.

172 Overall, the normalized NAI IC_{50} values of the ferret and mouse immune sera correlated very well
173 with coefficients values ranging from 0.33 to 0.78 (Figure 2 – figure supplement 5b).

174 **Association analysis reveals amino acid residue substitutions that strongly impact NAI**

175 NA of human influenza viruses is subject to antigenic drift, predominantly driven by the NAI activity
176 that is detectable in the host serum (Air et al., 1985; Yasuhara et al., 2019). There are a total of 102
177 amino acid differences between the head domains of the NAs that were used to generate the 44
178 ferret immune sera (Figure 3 - Figure supplement 1). These 102 variable amino acids in the N2 head
179 domain are predominantly exposed on the NA surface (Figure 3– figure supplement 2). To try to
180 identify which of these amino acid substitutions have a significant impact on NAI, we performed an
181 association analysis for each of the tested H6N2 viruses. For this analysis, the NAI IC_{50} value was
182 compared between groups of N2 sera according to the presence or absence of a substitution of any
183 of the 102 amino acid position that are different between the panel of 44 tested N2s against which
184 sera had been raised in ferrets. As a result, a p-value is obtained for each position that reflects its
185 possible impact on NAI (Figure 3a). The significance values higher than 1.3 ($p<0.05$) of representative
186 strains of the 4 antigenic groups were represented on the surface of N2 structure (Figure 3b). No
187 obvious antigenic patches, however, could be distinguished on the N2 NA surface.

188 A similar association analysis was performed using the NAI values obtained with the mouse NACHO
189 immune sera. The calculated p-values obtained from the mouse and ferret NAI data were in line with
190 each other (Figure 3 – figure supplement 3).

191 **Residues close to the catalytic pocket are more likely to impact NAI**

192 We next calculated the distance of every Cα atom of each amino acid present in the N2 structure
193 (PDB: 6BR6, from A/Perth/16/2009 NA) to each Cα of the variable amino acids. We then determined
194 the correlation of those distances with the p-values that were previously determined in the
195 association analysis. The resulting correlation coefficients (Tau values), indicate a similar pattern
196 among all 27 tested H6N2s (Figure 4a). When visualized on the N2 surface structure, the Tau values
197 revealed a geometrical distribution with the negative correlations being in closer proximity to the
198 catalytic pocket (Figure 4b). Similar data was obtained when mice sera were analyzed this way
199 (Figure 4 – figure supplement 1).

200 **Prediction of the N2 antigenicity based on a machine learning method**

201 The antigenic drift of human H3 HA has been extensively studied and modelled. (Meyer and Wilke,
202 2015; Smith et al., 2004; Westgeest et al., 2012; Wu et al., 2020). To model the NA drift observed in
203 our panel of N2 NAs, we first calculated the antigenic distances between the distinct NA sera, using a

204 similar approach as has been used to visualize the HA antigenic map (Cai et al., 2012). These
205 antigenic distances can be visualized using classical multidimensional scaling, and the resulting
206 antigenic map (Figure 5 – figure supplement 1a) revealed a distribution that is compatible with the
207 representation of phylogenetic distances (Figure 5 – figure supplement 1b).

208 Then, using the antigenic distances and a random forest method (RF), a model was built based on
209 amino acid sequence information. A similar model has been used by Yao *et al.* to predict the
210 antigenicity of H3 HA (Yao et al., 2017). Here, the optimized model was built using a combination of
211 25 randomly sampled data in 1500 decision trees. The resulting model generates predictive antigenic
212 distances that strongly correlate with the observed values (Figure 5a). The RF also enables scoring of
213 amino acid residues according to their importance in the decision trees. One measure of importance
214 can be defined as how early a change in a position is placed in the generated decision trees (mean
215 minimal depth). Another measure of importance is how much the standard error mean increases
216 when a variable is permuted. Finally, the prevalence of a variable amino acid in nodes of the decision
217 tree can also indicate its importance. Those importance scores were represented in a multi-way plot
218 (Figure 5b). The importance scores highlighted similar positions as previously determined in the
219 association study. Finally, we used NA sequences of recent seasonal influenza vaccine recommended
220 H3N2 strains to predict their antigenic distance relative to our panel of N2s, including 3 recent N2
221 NA components (from A/HongKong/45/2019, A/Tasmania/503/2020, and A/Darwin/6/2021) that
222 were not present in our data set. The predicted antigenic distances were plotted in the heatmap in a
223 red to blue scale, indicating high to low antigenic distance, respectively (Figure 5c). The RF clearly
224 reproduced the drift observed in AC2 versus AC1. The modelling also indicates that the antigenic
225 distance of the 3 recent N2s to their corresponding group 2 NAs is increasing (represented by the
226 dark blue turning light blue, from the A/Singapore/infimh-16-0019/2016 towards the
227 A/Darwin/6/2021 in G2) whereas their distance to group 4 NAs is decreasing (dark red becoming
228 yellow from the A/Singapore/infimh-16-0019/2016 towards the A/Darwin/6/2021 in G4).

229 **Discussion**

230 The sequence diversity of N2 protein derived from the 44 selected human H3N2 viruses isolated
231 between 2009 and 2017 allows to classify them in 4 major phylogenetic groups. Group 1 contains 22
232 N2 NAs, 4 of which were derived from vaccine recommended H3N2 strains: A/Perth/16/2009,
233 A/Texas/50/2012, A/Switzerland/9715293/2013, and A/Hong Kong/4801/2014. Phylogenetic group
234 2 comprises 15 N2 NAs, one of which is derived from a vaccine H3N2 recommended strain:
235 A/Singapore/INFIMH-16-0019/2016. The third phylogenetic group contains two NAs that are derived
236 from H3N2 strains that had been isolated in Helsinki in 2013. Remarkably, the NA sequence of these

237 two strains is closely related to that of H3N2s that circulated more than 15 years earlier (e.g. 99%
238 identity with NA of A/Sidney/5/1997). The fourth phylogenetic group is composed of NAs derived
239 from zoonotic cases with swine H3N2 strains isolated between 2012 and 2017. Swine-to-human
240 transmission of H3N2 viruses have occurred multiple times in the USA in 2012 and continue to be
241 detected at low frequency until to date (CDC, 2023; Elbe and Buckland-Merrett, 2017).

242 We assessed the antigenic diversity of the NA panel by generating 27 recombinant H6N2 viruses and
243 44 ferret NA immune sera produced by H1N2 priming followed by boosting with homologous
244 recombinant NA (NACHO; n = 42) or by reinfection with H1N2 (A/Estonia/91621/2015 and
245 A/Stockholm/15/2014). Most of the ferrets had detectable serum anti-N2 antibodies by day 14 after
246 infection with H1N2. Anti-NA antibody titers increased after a boost with non-adjuvanted
247 homologous recombinant CHO-produced soluble tetrameric NA suggesting that the use of
248 recombinant NA may boost naturally acquired anti-NA antibody responses in the human population.

249 The NAI activity of the ferret sera against 27 tested H6N2s reassortants revealed a pattern of
250 inhibition that largely coincides with the phylogenetic distances based on the NA head domain
251 sequences. In the tested panel of H6N2s, at least 4 major antigenic groups were identified. We
252 noted that H6N2 with Kan17 NA had a broader profile of inhibition than other H6N2 viruses from
253 group 2, being also inhibited by serum raised against NA from phylogenetic groups 3 and, to a lesser
254 extent, group 4. Additionally, the H6N2s Wis15 and Ala15 have an antigenic behaviour that is more
255 closely related to antigenic cluster 1, despite belonging to group 2 according to their phylogenetic
256 similarities. Based on the NAI panel, an association analysis was performed to try to identify amino
257 acid changes that affect NAI. It is interesting to note that the amino acid substitutions S245N and
258 S247T, combined with substitution P468H, were identified in this association analysis. Those
259 substitutions were described as major contributors of the NA antigenic drift that occurred in H3N2 in
260 2014 (Wan et al., 2019). NAs from A/Wisconsin/16/2015 and A/Alaska/251/2015 also have the
261 S245N and S247T substitutions and phylogenetically belong to group 2 NAs. However, those 2 NAs
262 lack the P468H mutation and are antigenically closer to group 1 NAs, confirming the requirement of
263 P468H combined with the S245N and S247T substitutions for this NA antigenic drift (Wan et al.,
264 2019). This observation suggests that NA antigenic drift may sometimes require a combination of
265 amino acid changes rather than single mutations. Wang and colleagues have very elegantly
266 demonstrated that N2 antigenic evolution is constrained by charge balances in an antigenic region,
267 which can partially explain the observation that NA amino acids can undergo co-evolution to result
268 in antigenic drift (Wang et al., 2021). Interestingly, NAs originated from H3N2 variants classified in
269 phylogenetic group 4 were antigenically closer to N2s belonging to phylogenetic group 1. This

270 suggest that the antigenic drift of recent NAs from group 2 increases the antigenic distance from the
271 N2s of swine origin.

272 Noteworthy, the analysis of the sera obtained from ferrets after infection shows that, despite the
273 lower homologous anti-NA titers, the inhibition pattern evaluated against 5 distinct H6N2s
274 (composed of at least one representative of each antigenic group) is in accordance with the
275 response obtained after boosting with recombinant protein. This suggests that a boost with
276 homologous recombinant soluble tetrameric NA does not alter the breadth of the antibody response
277 induced by H1N2 infection only.

278 NAI was also determined against 7 distinct H6N2 reassortant viruses using a panel of 43 anti-N2 NA
279 sera raised in mice by immunization with adjuvanted NACHOs. The observed NAI responses again
280 allowed clustering of the N2 NAs into 4 main antigenic groups, which correlates with data obtained
281 in ferrets. Studies in mice can thus offer a convenient alternative to the use of ferrets in future NA
282 antigenicity studies. This data also supports the hypothesis that there may be universal rules of
283 immunogen antigenicity and immunogenicity (Altman et al., 2015).

284 The determined K_M values of the H6N2 viruses used here, indicates that substrate affinity tends to
285 vary according to the phylogenetic relatedness of N2s. The N-glycosylation at position 245 was
286 previously described to be responsible for reducing N2 affinity for its substrate (Powell and Pekosz,
287 2020). Unlike group 2, which is primarily characterized by the presence of a N-glycan at position 245,
288 NAs from phylogenetic group 4 have a low K_M, indicating an increased affinity for substrate. This
289 result suggests that phylogenetic drift can be accompanied by changes in NA enzymatic properties.
290 Curiously, the Ala15, Wis15, and Kan17, despite having antigenic properties closer to group 1, still
291 have K_M values that are comparable to those of group 2 N2 NAs.

292 After the determination of NA antigenic distances, we used random forest modelling to estimate the
293 impact of amino acid changes on antigenic distances. We obtained a strong correlation of predicted
294 versus observed antigenic distances. However, it is important to note that the training dataset was
295 based on the 102 mutations present in our panel, limiting the predictions for other positions.
296 Furthermore, random forest enabled the classification of the variable amino acids according to
297 importance scores. It is important to highlight that co-occurring mutations in our panel (the ones
298 present in main branches of the phylogenetic tree) cannot be individually assessed by association
299 analysis or the random forest model. The individual weight of those mutations on NA drift remains
300 to be experimentally demonstrated. Interestingly the modelling could put in evidence the gradual
301 drift of recent N2s which were not present in the dataset (A/Hong Kong/45/2019,
302 A/Tasmania/503/2020, and A/Darwin/6/2021).

303 The protective potential of NA antigen against influenza has been underscored by multiple studies. It
304 is likely that NA will be included as a standard component of next generation influenza vaccines. The
305 difficulties of producing stable tetrameric NA may be overcome in the future thanks to protein
306 design or with the advent of mRNA-based vaccines (Catani et al., 2022; Chivukula et al., 2021; Ellis et
307 al., 2022). The antigenic modelling associated with sequence surveillance may increase our
308 predictive ability, highlighting major potential drifts and support NA antigen designs that may elicit
309 broader NAI responses compared to natural NA.

310 In summary, our study shows that immunization with recombinant N2 NA immunogen can boost
311 anti-NA serum antibody responses in ferrets that were primed by infection with an influenza virus
312 that carries the homologous NA. Prime by infection allowed to use non-adjuvanted NACHO in the
313 subsequent boost. At least 4 major antigenic groups could be distinguished in N2 NA derived from
314 human H3N2 viruses that were isolated between 2009 to 2017, and those antigenic groups
315 predominantly correspond with the phylogenetic relatedness of the N2 head domains. In addition,
316 the amino acid substitutions in close proximity of the NA catalytic pocket are more likely to affect
317 NAI patterns.

318 **Material and Methods**

319 **Rescue of H1N2 and H6N2 reassortants**

320 All reassortant H1N2 and H6N2 viruses included in the study were generated by reverse genetics,
321 with each reassortant expressing the targeted NA antigen, internal genes from A/Puerto
322 Rico/8/1934 H1N1 (PR8), and the HA from PR8 H1N1 or A/mallard/Sweden/81/2002 H6N1,
323 respectively. Briefly, HA and NA segments including non-coding regions were generated by custom
324 gene synthesis (Geneart AG), while PR8 internal segments were derived from a viral isolate as
325 previously published (Marsh and Tannock, 2005). All segments were cloned into a bi-directional
326 transcription plasmid derived from pUC57 (Genscript) including polymerase (Pol) I and Pol II
327 promoters, as previously described (Hoffmann et al., 2000), and the entire set of 8 plasmids was
328 used to transfect 293FT cells (Thermo Fisher Scientific) using Lipofectamine 2000 CD (Thermo Fisher
329 Scientific). Twenty-four hours after transfection, Madin-Darby Canine Kidney Cells (MDCK-) ATL cells
330 (ATCC) were added to the transfected cells in the presence of TPCK-treated trypsin (Sigma) to allow
331 influenza virus propagation. Cell culture supernatants containing influenza virus were harvested 7
332 days post-MDCK addition and blindly passaged in 8–10-day-old embryonated chicken eggs (Charles
333 River Laboratories, Inc.). Inoculated eggs were incubated at 37°C for 48 h, then cooled to 4°C for 12
334 h, prior to allantoic fluid harvest and clarification by low-speed centrifugation (3,000 rpm, 20 min).
335 For H6N2 viruses only, high-yield stocks were generated by an additional passage in eggs as
336 described above. Virus titers were determined by plaque assay on MDCK cells.

337 **Design and production of recombinant proteins**

338 The coding information of the NACHO proteins was cloned under the transcriptional control of the
339 CMV promoter in the pCDNA3.4 plasmid with a CD5 secretion signal, an amino-terminal His-tag and
340 the thrombin cleavage signal followed by tetrabrachion-NA. NACHOs were expressed in a
341 mammalian cell culture system as previously described with modifications (Catani et al., 2022).

342 **Animal experiments**

343 The ferret immunization experiment was conducted at Bioqual, Inc., MD (USA). The experiments
344 were approved by the Institutional Animal Care and Use Committee of the Bioqual (reference
345 number 17-021.6). Outbred 18-22 weeks old naïve male and female Fitch ferrets were obtained
346 from Triple F, PA (USA) and housed under specified pathogen-free conditions with food and water
347 *ad libitum*. Ferrets were primed on day 0 by intranasal challenge with influenza H1N2 reassortant
348 virus (1,000µl/dose, split evenly between nostrils). Four weeks after initial infection (day 28), ferrets
349 were immunized with 45 µg of NACHO (500µl/dose, intramuscularly, split evenly between hind

350 thighs) corresponding to homologous NA used in day 0 prime. Alternatively, and due to low yield of
351 selected recombinant NACHOs, ferrets were boosted on day 28 with 15 µg of homologous NACHO
352 (A/Perth/16/2009nib-64, A/Tasmania/1018/2015, A/Utah/11/2011, and A/West Virginia/17/2012)
353 or were inoculated with the same H1N2 reassortant virus used in the prime (A/Estonia/91621/2015
354 and A/Stockholm/15/2014). Sera from bleeds two weeks after the prime (day 14) and booster
355 vaccination (day 42) were tested for immunogenicity and seroconversion in serological assays.

356 The mouse immunization experiments were conducted according to the Belgian legislation (Belgian
357 Law 14/08/1986 and Belgium Royal Decree 06/04/2010) and European legislation on protection of
358 animals used for scientific purposes (EU directives 2010/63/EU and 86/609/EEC). Experimental
359 protocols were all approved by the Ethics Committee of the Vlaams Instituut voor Biotechnologie
360 (VIB), Ghent University, Faculty of Science (EC2019-035). Female BALB/c mice, aged 6–7 weeks, were
361 purchased from Charles River. The mice were housed in a specified pathogen-free animal house with
362 food and water *ad libitum*. Animals were immunized intramuscularly in the right quadriceps.
363 Immunization was performed with 50 µl containing 1 µg of recombinant protein (tetrabrachion
364 stabilized NAs, referred to as NACHOs). All, except A/West Virginia/17/2012 NACHOs were used as
365 immunogens in mice. All immunizations were adjuvanted with a 1:1 volume of AF03 (25 µl of antigen
366 in PBS + 25 µl of AF03 per dose) (Caillet et al., 2010).

367 Two or three weeks after the boost immunization, mice were humanely sacrificed with an
368 anaesthetic overdose of Nembutal (6 mg per mouse) and bled retro-orbitally. The obtained blood
369 samples were incubated for 30 min at 37°C to allow clotting, which was followed by centrifugation at
370 10,500 g for 5 minutes. The supernatant (the serum) was recovered and submitted to a second
371 centrifugation at 10,500 g for 5 minutes. Cleared sera were stored at -20°C before use in serological
372 assays.

373 **ELISA**

374 Anti-tetNA IgG levels in mouse and ferret sera were determined by capture ELISA using tetNAs in
375 Pierce™ nickel-coated plates (cat. # 15442). Recombinant proteins were diluted in DPBS (Life
376 technologies cat. # 14040-182) (tetNA was diluted to 0.5 µg/ml). Then, 50 µl of the coating antigen
377 solutions was added to each well and the plate was incubated at room temperature for 1 h on a
378 shaking platform. The wells of the plates were then washed 3 times with PBS-T (Sigma cat. # P3563-
379 10PAK) and blocked for 1h with 1% BSA (for the mouse sera) or 10% milk (for the ferret sera) in
380 DPBS. After blocking, the wells of the plates were washed once with PBS-T and incubated with a 3-
381 fold serial dilution, starting at a 1/100 dilution, of serum in DPBS, 0.5% BSA, 0.05% tween-20 for 2h
382 at room temperature on a shaking platform. The wells of the plates were then washed 5 times with

383 PBS-T and incubated with a 1:5000 dilution of anti-mouse IgG-HRP (GE healthcare cat. # NA931-1ml),
384 or with a 1:100000 dilution of anti-ferret IgG-HRP (Abcam cat. # 112770) in DPBS, 0.5% BSA, 0.05%
385 Tween-20. The 3,3',5,5'-tetramethylbenzidine (TMB) substrate (BD cat. # 555214) was added after 3
386 washes with PBS-T and the reaction was stopped after 5 min by addition of 50 µl of 1 M H_2SO_4. The
387 optical density (O.D.) in each well was determined at 450 nm and, as a reference, 655 nm using an
388 iMark™ Microplate Absorbance Reader (Bio-rad). The end point titer was determined for each serum
389 sample by scoring the dilution that resulted in an O.D. that was equal to or 2 times higher than the
390 background O.D. obtained from pre-immune control sera dilution series.

391 **Enzyme-linked lectin assay to determine neuraminidase inhibition titers**

392 Fetuin (Sigma cat. # F3385) was diluted into coating buffer (KPL cat. # 50-84-01) to a concentration
393 of 25 µg/ml and 50 µl was added to the wells of Nunc MaxiSorp™ plates (Thermofisher cat. # 44-
394 2404-21), which were incubated overnight at 4°C. The coated plates were then washed 3 times with
395 PBS-T (Sigma cat. # P3563-10PAK) and incubated overnight with 60 µl of a dilution of H6N2 and 60 µl
396 of 2-fold serial dilution of serum, starting at a 1/20 dilution, in sample buffer (1X MES VWR cat. #
397 AAJ61979-AP: 20mM $CaCl_2$, 1% BSA, 0.5% Tween-20). These dilutions of the H6Nx viruses
398 correspond to the 70% maximum activity of NA from the respective viruses as determined in the
399 ELLA assay. Fetuin-coated plates were then washed 3 times with PBS-T and incubated for 1 h with a
400 solution of PNA-HRP (cat. # L6135-1MG, Sigma) at 5 µg/ml in conjugate diluent (MES pH 6.5, 20 mM
401 CaCl2, 1% BSA). The plates were washed 3 times with PBS-T, TMB substrate was added and then the
402 plates were incubated for 5 minutes before the reaction was stopped by the addition of 50 µl of 1 M
403 H_2SO_4. The optical density was measured at 450 nm and, as a reference, 655 nm in an iMark™
404 Microplate Absorbance Reader (Bio-rad). Half maximum inhibitory concentrations (IC_{50}) values were
405 determined by non-linear regression analysis (GraphPad Prism software).

406 **NA Enzyme Kinetics Assay**

407 The enzymatic activity of NACHOs and H6N2s was determined with the fluorogenic small substrate
408 4-methylumbelliferyl)-α-d-*N*-acetylneuraminic acid (MUNANA) as previously described (Marathe et
409 al., 2013). First H6N2 dilutions were tested to ensure that MUNANA conversion into 4-
410 methylumbelliferone (4-MU) generated fluorescence over time at a linear ratio. Ten microliters of
411 1 mM of MUNANA (Sigma cat # M8639) in 200 mM sodium acetate buffer (pH 6.5) containing 2 mM
412 $CaCl_2$ and 1% butanol was incubated with 40 µl of PBS solution containing viral dilution. Conversion
413 to 4-MU was monitored every 2 min for 1 h using a BMG Fluostar OPTIMA reader (excitation at
414 365 nm and emission determined at 450 nm). Second, using the selected dilution of virus, the assay
415 was repeated with dilutions of MUNANA ranging from 2.5 to 100 µM. A standard curve with 800 to

416 25 pmoles/well of 4-MU (Sigma cat # M1508) was used to extrapolate the molar conversion of
417 MUNANA. K_M was calculated using GraphPad Prism version 8.4.3.

418 **Association study**

419 For the association analysis, under the assumption of homogeneous genetic relatedness among the
420 selected H3N2 virus strains, a simple linear regression model for mutation-trait association analysis
421 was fitted to the data for each H6N2 separately. The significance values were calculated by
422 comparing IC_{50} values of sera that were classified into 2 groups according to the presence or absence
423 of variation in the amino acid of reference Tex12 sequence.

424 **Correlations with distances from the NA catalytic pocket**

425 Tau values were determined by correlating distances with significance values obtained from the
426 association analysis or the importance scores obtained from machine learning. A similar method was
427 described by Meyer *et al*. to define geometrical constraints of HA evolution (Meyer and Wilke,
428 2015). Briefly, the relative distances of amino acids were calculated based on the structure of
429 A/Perth/2009 (H3N2) NA (PDB: 6BR6) (Hadházi et al., 2018). The distances were calculated from
430 each Cα to every other Cα. The distances from every residue to the 98 variable residues that are
431 present in the panel of N2s and 6BR6 structure were then correlated with the significance values
432 that were obtained in the association analysis, or importance scores obtained in the machine
433 learning. Correlation coefficients were visualized on the structure of N2 NA derived from pandemic
434 A/RI/5+/1957 H2N2 virus (PDB: 4H53)(Vavricka et al., 2013) using Chimera 1.14.

435 **Random Forest algorithm**

436 The Random Forest algorithm was adapted from (Yao et al., 2017). Briefly, the non-conserved
437 positions in the multiple sequence alignment of N2 head domain amino acid sequences of all tested
438 N2s were selected. The feature matrix (X) was created by assessing matches/mismatches on each
439 non-conserved position for each pair of N2 head domain amino acid sequences as:

$$X = \begin{array}{c|cccc} & X_1 & X_2 & \cdots & X_m \\ \hline V_1V_2 & 0 & 1 & \dots & 1 \\ \vdots & \vdots & \vdots & \dots & \vdots \\ V_1V_n & 1 & 0 & \dots & 1 \\ \vdots & \vdots & \vdots & \dots & \vdots \\ V_{n-1}V_n & 1 & 0 & \dots & 1 \end{array}$$

440 where X_i represents the non-conserved positions in the multiple sequence alignment
441 m is the number of non-conserved positions (102 in total)
442 V_i represents the N2 head domain sequence for each tested NA

n is the number of tested sera (44 in total)

0 represents a match, 1 represents a mismatch in the alignment

The response vector (Y) is composed of the antigenic distances for each pair of tested sera. These antigenic distances were determined based on NAI, similarly to the method used to determine HI based immunogenic distances that was described by Cai *et al*. In summary, the distances between sera was calculated as $\frac{1}{n}\sum_{t=1}^{n}|d[t,i]-d[i,t]|$, which represent average distances between 2 serum samples among all tested H6N2s (Cai et al., 2012). We applied the random forest function from the randomForest package in R to construct the model. We set the bootstrapping (tree) number to 1500 and the number of features to 25 for each tree. Accuracy was determined as the root-mean-square error (RMSE), calculated using the RMSE function from the yardstick package in R.

Additionally, predicted antigenic distances of the out-of-bag samples were compared to the observed distances by fitting a linear model and calculating the R^2 value. To calculate the importance of each feature (X_i), the following metrics were calculated using the measure importance function of the randomForestExplainer package in R:

- mean minimal depth: mean of the depths of the node in each tree that splits on this feature and is the closest to the root of the tree (minimal depth). The lower, the more important the feature since a low depth means that many observations are divided into groups based on this feature.
- mse decrease: mean decrease of accuracy in predictions on out of bag samples when the feature is excluded from the model. The higher, the more important the feature.
- number of nodes: total number of nodes in the forest that use the feature for splitting. The higher, the more important the feature.

466 **Acknowledgements**

467 We gratefully acknowledge all data contributors, i.e., the Authors and their Originating
468 laboratories responsible for obtaining the specimens, and their Submitting laboratories for
469 generating the genetic sequence and metadata and sharing via the GISAID Initiative, on which
470 this research is based.

471 We are grateful to the animal caretakers of the animal house at the VIB-UGent Center for
472 Inflammation Research.

473 **Competing interests**

474 XS reports grants from Sanofi Vaccines. GCG, TS, RG, JH, JC, IVU, TF, SS, SR, LR, and TUV are or
475 were Sanofi employees and may hold shares and/or stock options in the company.

476 **Disclosure of funding sources**

477 This work was funded by Sanofi Vaccines.

478 **Author Contributions**

479 JPPC, TY, AS, IVU, TF, RG, JH, SS, SR, LL and JC performed experimental work. JPPC, TY, AS, RG,
480 GCG, TUV, and XS designed the experiments, analyzed and interpreted the data. JM and MV
481 analyzed the data. JPPC and XS wrote the manuscript and are accountable for accuracy and
482 integrity of the work. All authors proofread and critically reviewed the manuscript.

483 **References**

484 Air GM, Els MC, Brown LE, Laver WG, Webster RG. 1985. Location of antigenic sites on the three-
485 dimensional structure of the influenza N2 virus neuraminidase. *Virology* **145**:237–248.
486 doi:10.1016/0042-6822(85)90157-6
487 Altman MO, Bennink JR, Yewdell JW, Herrin BR. 2015. Lamprey VLRB response to influenza virus
488 supports universal rules of immunogenicity and antigenicity. *eLife* **4**:e07467.
489 doi:10.7554/eLife.07467
490 Bedford T, Suchard MA, Lemey P, Dudas G, Gregory V, Hay AJ, McCauley JW, Russell CA, Smith DJ,
491 Rambaut A. 2014. Integrating influenza antigenic dynamics with molecular evolution. *eLife*
492 **3**:e01914. doi:10.7554/eLife.01914
493 Belongia EA, Simpson MD, King JP, Sundaram ME, Kelley NS, Osterholm MT, McLean HQ. 2016.
494 Variable influenza vaccine effectiveness by subtype: a systematic review and meta-analysis
495 of test-negative design studies. *The Lancet Infectious Diseases* **16**:942–951.
496 doi:10.1016/S1473-3099(16)00129-8
497 Bien J, Tibshirani R. 2011. Hierarchical Clustering With Prototypes via Minimax Linkage. *J Am Stat*
498 *Assoc* **106**:1075–1084.
499 Cai Z, Zhang T, Wan X-F. 2012. Antigenic Distance Measurements for Seasonal Influenza Vaccine
500 Selection. *Vaccine* **30**:448–453. doi:10.1016/j.vaccine.2011.10.051
501 Caillet C, Piras F, Bernard M-C, de Montfort A, Boudet F, Vogel FR, Hoffenbach A, Moste C, Kusters I.
502 2010. AF03-adjuvanted and non-adjuvanted pandemic influenza A (H1N1) 2009 vaccines
503 induce strong antibody responses in seasonal influenza vaccine-primed and unprimed mice.
504 *Vaccine* **28**:3076–3079. doi:10.1016/j.vaccine.2010.02.050
505 Catani JPP, Job ER, Ysenbaert T, Smet A, Ray S, LaRue L, Stegalkina S, Barro M, Vogel TU, Saelens X.
506 2022. Pre-existing antibodies directed against a tetramerizing domain enhance the immune
507 response against artificially stabilized soluble tetrameric influenza neuraminidase. *npj*
508 *Vaccines* **7**:1–9. doi:10.1038/s41541-022-00435-7
509 CDC. 2023. Novel Influenza A Virus Infections. *Fluview*.
510 https://gis.cdc.gov/grasp/fluview/Novel_Influenza.html
511 Chen YQ, Wohlbold TJ, Zheng NY, Huang M, Huang Y, Neu KE, Lee J, Wan H, Rojas KT, Kirkpatrick E,
512 Henry C, Palm AKE, Stamper CT, Lan LYL, Topham DJ, Treanor J, Wrammert J, Ahmed R,
513 Eichelberger MC, Georgiou G, Krammer F, Wilson PC. 2018. Influenza Infection in Humans
514 Induces Broadly Cross-Reactive and Protective Neuraminidase-Reactive Antibodies. *Cell*
515 **173**:417-429.e10. doi:10.1016/j.cell.2018.03.030
516 Chivukula S, Plitnik T, Tibbitts T, Karve S, Dias A, Zhang D, Goldman R, Gopani H, Khanmohammed A,
517 Sarode A, Cooper D, Yoon H, Kim Y, Yan Y, Mundle ST, Groppo R, Beauvais A, Zhang J,
518 Anosova NG, Lai C, Li L, Ulinski G, Piepenhagen P, DiNapoli J, Kalnin KV, Landolfi V,
519 Swearingen R, Fu T-M, DeRosa F, Casimiro D. 2021. Development of multivalent mRNA
520 vaccine candidates for seasonal or pandemic influenza. *NPJ Vaccines* **6**:153.
521 doi:10.1038/s41541-021-00420-6
522 Couch RB, Atmar RL, Franco LM, Quarles JM, Wells J, Arden N, Niño D, Belmont JW. 2013. Antibody
523 Correlates and Predictors of Immunity to Naturally Occurring Influenza in Humans and the
524 Importance of Antibody to the Neuraminidase. *The Journal of Infectious Diseases* **207**:974–
525 981. doi:10.1093/infdis/jis935
526 Cox RJ. 2013. Correlates of protection to influenza virus, where do we go from here? *Hum Vaccin*
527 *Immunother* **9**:405–408. doi:10.4161/hv.22908
528 de Vries E, Du W, Guo H, de Haan CAM. 2020. Influenza A Virus Hemagglutinin–Neuraminidase–
529 Receptor Balance: Preserving Virus Motility. *Trends in Microbiology* **28**:57–67.
530 doi:10.1016/j.tim.2019.08.010
531 Deroo T, Min Jou W, Fiers W. 1996. Recombinant neuraminidase vaccine protects against lethal
532 influenza. *Vaccine* **14**:561–569. doi:10.1016/0264-410X(95)00157-V

533 Eickhoff TC, Meiklejohn G. 1969. Protection against Hong Kong influneza by adjuvant vaccine
534 containing A2-Ann Arbor-67. *Bull World Health Organ* **41**:562–563.
535 Elbe S, Buckland-Merrett G. 2017. Data, disease and diplomacy: GISAID's innovative contribution to
536 global health. *Global Challenges* **1**:33–46. doi:10.1002/gch2.1018
537 Ellis D, Lederhofer J, Acton OJ, Tsybovsky Y, Kephart S, Yap C, Gillespie RA, Creanga A, Olshefsky A,
538 Stephens T, Pettie D, Murphy M, Sydeman C, Ahlrichs M, Chan S, Borst AJ, Park Y-J, Lee KK,
539 Graham BS, Veesler D, King NP, Kanekiyo M. 2022. Structure-based design of stabilized
540 recombinant influenza neuraminidase tetramers. *Nat Commun* **13**:1825.
541 doi:10.1038/s41467-022-29416-z
542 Hadházi Á, Li L, Bailly B, Maggioni A, Martin G, Dirr L, Dyason JC, Thomson RJ, Gao GF, Borbás A, Ve T,
543 Pascolutti M, von Itzstein M. 2018. A Sulfonozanamivir Analogue Has Potent Anti-influenza
544 Virus Activity. *ChemMedChem* **13**:785–789. doi:10.1002/cmdc.201800092
545 Hoffmann E, Neumann G, Kawaoka Y, Hobom G, Webster RG. 2000. A DNA transfection system for
546 generation of influenza A virus from eight plasmids. *Proc Natl Acad Sci U S A* **97**:6108–6113.
547 doi:10.1073/pnas.100133697
548 Jester BJ, Uyeki TM, Jernigan DB. 2020. Fifty Years of Influenza A(H3N2) Following the Pandemic of
549 1968. *Am J Public Health* **110**:669–676. doi:10.2105/AJPH.2019.305557
550 Krammer F, Fouchier RAM, Eichelberger MC, Webby RJ, Shaw-Saliba K, Wan H, Wilson PC, Compans
551 RW, Skountzou I, Monto AS. 2018. NAction! How Can Neuraminidase-Based Immunity
552 Contribute to Better Influenza Virus Vaccines? *mBio* **9**:e02332-17. doi:10.1128/mBio.02332-
553 17
554 Leneva IA, Roberts N, Govorkova EA, Goloubeva OG, Webster RG. 2000. The neuraminidase inhibitor
555 GS4104 (oseltamivir phosphate) is efficacious against A/Hong Kong/156/97 (H5N1) and
556 A/Hong Kong/1074/99 (H9N2) influenza viruses. *Antiviral Res* **48**:101–115.
557 doi:10.1016/s0166-3542(00)00123-6
558 Maier HE, Nachbagauer R, Kuan G, Ng S, Lopez R, Sanchez N, Stadlbauer D, Gresh L, Schiller A,
559 Rajabhathor A, Ojeda S, Guglia AF, Amanat F, Balmaseda A, Krammer F, Gordon A. 2019. Pre-
560 existing anti-neuraminidase antibodies are associated with shortened duration of influenza
561 A (H1N1)pdm virus shedding and illness in naturally infected adults. *Clinical Infectious*
562 *Diseases*. doi:10.1093/cid/ciz639
563 Marathe BM, Lévêque V, Klumpp K, Webster RG, Govorkova EA. 2013. Determination of
564 Neuraminidase Kinetic Constants Using Whole Influenza Virus Preparations and Correction
565 for Spectroscopic Interference by a Fluorogenic Substrate. *PLOS ONE* **8**:e71401.
566 doi:10.1371/journal.pone.0071401
567 Marsh G, Tannock G. 2005. The role of reverse genetics in the development of vaccines against
568 respiratory viruses. *Expert Opin Biol Ther* **5**:369–380. doi:10.1517/14712598.5.3.369
569 Matrosovich MN, Matrosovich TY, Gray T, Roberts NA, Klenk H-D. 2004. Neuraminidase Is Important
570 for the Initiation of Influenza Virus Infection in Human Airway Epithelium. *Journal of Virology*
571 **78**:12665–12667. doi:10.1128/jvi.78.22.12665-12667.2004
572 Memoli MJ, Shaw PA, Han A, Czajkowski L, Reed S, Athota R, Bristol T, Fargis S, Risos K, Powers JH,
573 Davey RT, Taubenberger JK. 2016. Evaluation of Antihemagglutinin and Antineuraminidase
574 Antibodies as Correlates of Protection in an Influenza A/H1N1 Virus Healthy Human
575 Challenge Model. *mBio* **7**:e00417-16. doi:10.1128/mBio.00417-16
576 Meyer AG, Wilke CO. 2015. Geometric Constraints Dominate the Antigenic Evolution of Influenza
577 H3N2 Hemagglutinin. *PLOS Pathogens* **11**:e1004940. doi:10.1371/journal.ppat.1004940
578 Monto ArnoldS, Kendal AlanP. 1973. EFFECT OF NEURAMINIDASE ANTIBODY ON HONG KONG
579 INFLUENZA. *The Lancet*, Originally published as Volume 1, Issue 7804 **301**:623–625.
580 doi:10.1016/S0140-6736(73)92196-X
581 Monto AS, Petrie JG, Cross RT, Johnson E, Liu M, Zhong W, Levine M, Katz JM, Ohmit SE. 2015.
582 Antibody to influenza virus neuraminidase: An independent correlate of protection. *Journal*
583 *of Infectious Diseases* **212**:1191–1199. doi:10.1093/infdis/jiv195

584 Nachbagauer R, Choi A, Hirsh A, Margine I, Iida S, Barrera A, Ferres M, Albrecht RA, García-Sastre A,
585 Bouvier NM, Ito K, Medina RA, Palese P, Krammer F. 2017. Defining the antibody cross-
586 reactome directed against the influenza virus surface glycoproteins. *Nat Immunol* **18**:464–
587 473. doi:10.1038/ni.3684
588 Ng S, Nachbagauer R, Balmaseda A, Stadlbauer D, Ojeda S, Patel M, Rajabhathor A, Lopez R, Guglia
589 AF, Sanchez N, Amanat F, Gresh L, Kuan G, Krammer F, Gordon A. 2019. Novel correlates of
590 protection against pandemic H1N1 influenza A virus infection. *Nature Medicine* **25**:962–967.
591 doi:10.1038/s41591-019-0463-x
592 Palese P, Tobita K, Ueda M, Compans RW. 1974. Characterization of temperature sensitive influenza
593 virus mutants defective in neuraminidase. *Virology* **61**:397–410. doi:10.1016/0042-
594 6822(74)90276-1
595 Potter BI, Kondor R, Hadfield J, Huddleston J, Barnes J, Rowe T, Guo L, Xu X, Neher RA, Bedford T,
596 Wentworth DE. 2019. Evolution and rapid spread of a reassortant A(H3N2) virus that
597 predominated the 2017–2018 influenza season. *Virus Evol* **5**:vez046. doi:10.1093/ve/vez046
598 Powell H, Pekosz A. 2020. Neuraminidase antigenic drift of H3N2 clade 3c.2a viruses alters virus
599 replication, enzymatic activity and inhibitory antibody binding. *PLOS Pathogens*
600 **16**:e1008411. doi:10.1371/journal.ppat.1008411
601 Rajendran M, Nachbagauer R, Ermler ME, Bunduc P, Amanat F, Izikson R, Cox M, Palese P,
602 Eichelberger M, Krammer F. 2017. Analysis of anti-influenza virus neuraminidase antibodies
603 in children, adults, and the elderly by ELISA and enzyme inhibition: Evidence for original
604 antigenic sin. *mBio* **8**. doi:10.1128/mBio.02281-16
605 Rosu ME, Kok A, Bestebroer TM, de Meulder D, Verveer EP, Pronk MR, Dekker LJM, Luider TM,
606 Richard M, van den Brand JMA, Fouchier RAM, Herfst S. 2022. Contribution of
607 Neuraminidase to the Efficacy of Seasonal Split Influenza Vaccines in the Ferret Model. *J*
608 *Virol* **96**:e0195921. doi:10.1128/jvi.01959-21
609 Smith DJ, Lapedes AS, de Jong JC, Bestebroer TM, Rimmelzwaan GF, Osterhaus ADME, Fouchier
610 RAM. 2004. Mapping the antigenic and genetic evolution of influenza virus. *Science*
611 **305**:371–376. doi:10.1126/science.1097211
612 Uyeki TM, Hui DS, Zambon M, Wentworth DE, Monto AS. 2022. Influenza. *The Lancet* **400**:693–706.
613 doi:10.1016/S0140-6736(22)00982-5
614 Vavricka CJ, Liu Y, Kiyota H, Sriwilaijaroen N, Qi J, Tanaka K, Wu Y, Li Q, Li Y, Yan J, Suzuki Y, Gao GF.
615 2013. Influenza neuraminidase operates via a nucleophilic mechanism and can be targeted
616 by covalent inhibitors. *Nature Communications* **4**. doi:10.1038/ncomms2487
617 Viboud C, Grais RF, Lafont BAP, Miller MA, Simonsen L. 2005. Multinational Impact of the 1968 Hong
618 Kong Influenza Pandemic: Evidence for a Smoldering Pandemic. *The Journal of Infectious*
619 *Diseases* **192**:233–248. doi:10.1086/431150
620 Wan H, Gao J, Yang H, Yang S, Harvey R, Chen YQ, Zheng NY, Chang J, Carney PJ, Li X, Plant E, Jiang L,
621 Couzens L, Wang C, Strohmeier S, Wu WW, Shen RF, Krammer F, Cipollo JF, Wilson PC,
622 Stevens J, Wan XF, Eichelberger MC, Ye Z. 2019. The neuraminidase of A(H3N2) influenza
623 viruses circulating since 2016 is antigenically distinct from the A/Hong Kong/4801/2014
624 vaccine strain. *Nature Microbiology* **4**:2216–2225. doi:10.1038/s41564-019-0522-6
625 Wan H, Qi L, Gao J, Couzens LK, Jiang L, Gao Y, Sheng Z-M, Fong S, Hahn M, Khurana S, Taubenberger
626 JK, Eichelberger MC. 2018. Comparison of the Efficacy of N9 Neuraminidase-Specific
627 Monoclonal Antibodies against Influenza A(H7N9) Virus Infection. *Journal of Virology*
628 **92**:e01588-17. doi:10.1128/JVI.01588-17
629 Wang Y, Lei R, Nourmohammad A, Wu NC. 2021. Antigenic evolution of human influenza H3N2
630 neuraminidase is constrained by charge balancing. *eLife* **10**:e72516. doi:10.7554/eLife.72516
631 Weiss CD, Wang W, Lu Y, Billings M, Eick-Cost A, Couzens L, Sanchez JL, Hawksworth AW, Seguin P,
632 Myers CA, Forshee R, Eichelberger MC, Cooper MJ. 2019. Neutralizing and Neuraminidase
633 Antibodies Correlate With Protection Against Influenza During a Late Season A/H3N2

634 Outbreak Among Unvaccinated Military Recruits. *Clinical Infectious Diseases* 1–7.
635 doi:10.1093/cid/ciz1198
636 Westgeest KB, de Graaf M, Fourment M, Bestebroer TM, van Beek R, Spronken MIJ, de Jong JC,
637 Rimmelzwaan GF, Russell CA, Osterhaus ADME, Smith GJD, Smith DJ, Fouchier RAM. 2012.
638 Genetic evolution of the neuraminidase of influenza A (H3N2) viruses from 1968 to 2009 and
639 its correspondence to haemagglutinin evolution. *J Gen Virol* **93**:1996–2007.
640 doi:10.1099/vir.0.043059-0
641 Wohlbold TJ, Podolsky KA, Chromikova V, Kirkpatrick E, Falconieri V, Meade P, Amanat F, Tan J,
642 Tenoever BR, Tan GS, Subramaniam S, Palese P, Krammer F. 2017. Broadly protective murine
643 monoclonal antibodies against influenza B virus target highly conserved neuraminidase
644 epitopes. *Nature Microbiology* **2**:1415–1424. doi:10.1038/s41564-017-0011-8
645 Wu NC, Otwinowski J, Thompson AJ, Nycholat CM, Nourmohammad A, Wilson IA. 2020. Major
646 antigenic site B of human influenza H3N2 viruses has an evolving local fitness landscape. *Nat*
647 *Commun* **11**:1233. doi:10.1038/s41467-020-15102-5
648 Yao Y, Li X, Liao B, Huang L, He P, Wang F, Yang Jiasheng, Sun H, Zhao Y, Yang Jialiang. 2017.
649 Predicting influenza antigenicity from Hemagglutintin sequence data based on a joint
650 random forest method. *Sci Rep* **7**:1545. doi:10.1038/s41598-017-01699-z
651 Yasuhara A, Yamayoshi S, Kiso M, Sakai-Tagawa Y, Koga M, Adachi E, Kikuchi T, Wang IH, Yamada S,
652 Kawaoka Y. 2019. Antigenic drift originating from changes to the lateral surface of the
653 neuraminidase head of influenza A virus. *Nature Microbiology* **4**:1024–1034.
654 doi:10.1038/s41564-019-0401-1
655 Yen H-L, Herlocher LM, Hoffmann E, Matrosovich MN, Monto AS, Webster RG, Govorkova EA. 2005.
656 Neuraminidase Inhibitor-Resistant Influenza Viruses May Differ Substantially in Fitness and
657 Transmissibility. *Antimicrob Agents Chemother* **49**:4075–4084. doi:10.1128/AAC.49.10.4075-
658 4084.2005
659

660

661 **Table S1. Specific activity of the recombinant NACHOs.**

H3N2 strain NA source	Specific Activity nmole/min.µg
A/Stockholm/32/2014	9,62
A/Switzerland/9715293/2013	6,52
A/Hong Kong/4801/2014	4,13
A/Paris/2379/2014	2,42
A/Texas/50/2012	5,21
A/Stockholm/14/2012	2,42
A/Tehran/996/2012	8,46
A/Victoria/361/2011	2,71
A/New_Castle/67/2016	3,22
A/Estonia/91621/2015	5,3
A/Ankara/2396/2015	2,62
A/Stockholm/15/2014	1,14
A/Dakar/14/2014	2,37
A/PortoAlegre/Lacenrs-2376/2014	2,55
A/Utah/11/2011	1,40
A/Hokkaido/IOH079/2011	0,84
A/Gambia/2012	1,60
A/Hanoi/Eli15597/2015	3,29
A/XinJiang-Tianshan/1411/2012	0,27
A/Perth/16/2009nib-64	5,3
A/Tasmania/1018/2015	27,48
A/NewCaledonia/23/2016	8,55
A/Alaska/251/2015	4,29
A/Hatay/4990/2016	5,83
A/Tennessee/18/2017	5,99
A/Singapore/Infimh160019/2016	8,01
A/Brisbane/273/2016	6,94
A/Poland/19b/2017	5,81
A/Wisconsin/16/2015	1,40
A/Indiana/08/2011	4,13
A/Hong-Kong/3089/2017	6,17
A/Nagano/2153/2017	2,29
A/Sweden/3/2017	2,76
A/Catalonia/9503s/2017	1,31
A/Moramanga/1907/2017	2,09
A/Heilongjiang_Xiangyan/1134/2011	6,61
A/Helsinki/823/2013	6,53
A/Helsinki/941/2013	7,02
A/Ohio/13/2017	2,59

A/Ohio/62/2012	4,28
A/Ontario/RV3236/2016	3,89
A/Indiana/18/2017	4,27
A/Minnesota/11/2010	4,25

662

663 **Table S2. H6N2 reassortant viruses used in the ELLA assay.**

H6Nx reassortant(*)	Titer (PFU/ml)	dilution to 70% max activity (ELLA)	K_M (MUNANA)
A/Ohio/62/2012 (Ohi12)	2.00E+08	2269.7	20.7
A/Indiana/08/2011 (Ind11)	2.50E+08	750.9	40.1
A/Ohio/13/2017 (Ohi17)	3.00E+08	521.5	33.5
A/Ontario/Rv3236/2016 (Ont16)	1.75E+08	504.1	31.5
A/Minnesota/11/2010 (Min10)	2.00E+08	1031.4	41.3
A/Helsinki/823/2013 (Hel823)	1.50E+08	155.2	45.9
A/Helsinki/941/2013 (Hel941)	3.50E+08	341.6	45.3
A/Nagano/2153/2017 (Nag17)	2.50E+08	213.6	97.8
A/Singapore/Infimh-16-0019/2016 (Sin16)	6.50E+07	257.1	93.3
A/Hong_Kong/3089/2017 (HK17)	2.00E+08	301.6	85.2
A/Sweden/3/2017 (Swe17)	6.00E+08	97	71.5
A/Moramanga/1907/2017 (Mor17)	1.40E+08	151.4	56.8
A/Kansas/14/2017 (Kan17)	2.50E+08	249	108.7
A/Wisconsin/16/2015 (Wis15)	2.00E+08	63.3	79.6
A/Gambia/G0071436/2012 (Gam12)	2.50E+08	331.5	63.6
A/Heilongjiang-Xiangyang/1134/2011 (Hei11)	2.10E+08	195.6	31.1
A/Perth/16/2009 (Per09)	3.20E+08	630.8	56.4
A/Newcastle/67/2016 (NCas16)	1.50E+08	150.4	48.5
A/Tasmania/1018/2015 (Tas15)	1.70E+08	139.5	54.8
A/Hanoi/Eli15597/2015 (Han15)	1.40E+08	94.6	82.2
A/Alaska/251/2015 (Ala15)	4.50E+08	93.7	144.8
A/Estonia/91621/2015 (Est15)	2.00E+08	281.9	62.1
A/Victoria/361/2011 (Vic11)	3.00E+08	570.3	51.1
A/Utah/11/2011 (Uta11)	2.50E+08	356.3	51.9
A/Switzerland/9715293/2013 (Swi13)	2.70E+08	160.8	64
A/Hong Kong/4801/2014 (HK14)	4.00E+07	106.3	54.7
A/Texas/50/2012 (Tex12)	2.00E+08	276.6	45.1

664

665 *Name of the virus from which the N2 NA in H6N2 reassortant virus was derived. The short name as
666 used in the manuscript text is mentioned between brackets.

667

668 **Table S3 . NAI titers against H6N2 viruses of ferret sera obtained after the boost (Part I of II).**

Sera	Swi13	HK14	Tex12	Vic11	Ncas16	Est15	Uta11	Gam12	Han15	Hei11	Per09	Tas15	Ala15
A/Switzerland/9715293/2013	**9333.0**	6833.5	10301.6	2442.3	1489.8	5530.4	1460.6	3489.9	5253.8	1510.9	1899.6	1649.9	1812.3
A/Hong_Kong/4801/2014	7527.5	**10566.4**	14983.0	2559.1	4579.4	7944.5	3590.3	7065.0	4798.3	1971.2	2522.9	3842.2	4980.9
A/Texas/50/2012	10751.3	10397.6	**8843.5**	2089.6	740.9	3821.0	902.1	1519.1	1453.1	1112.9	2506.5	835.8	1490.8
A/Victoria/361/2011(Ivr-165)	16804.7	11568.3	11892.0	**3863.7**	1868.9	3480.4	2250.0	670.9	3963.3	1379.1	2888.7	883.1	1531.9
A/Newcastle/67/2016	7647.2	9702.6	5244.0	1056.9	**4218.8**	2295.9	5477.0	821.2	1515.9	1254.3	1304.0	1253.1	1021.6
A/Estonia/91621/2015	1277.1	1379.5	911.1	387.1	290.5	**2832.9**	277.9	335.3	225.6	272.5	193.3	217.2	70.9
A/Utah/11/2011	6121.8	6591.4	6253.2	3392.5	1570.0	3727.5	**2893.7**	1294.7	2496.3	4050.7	2196.7	376.0	869.2
A/Gambia/G0071436/2012	5513.7	6192.0	5040.0	1226.5	1492.3	6342.9	772.9	**730.2**	863.5	1810.2	1399.4	836.9	888.0
A/Hanoi/Eli15597/2015	4635.2	8150.5	6232.1	872.7	1617.0	7192.3	1023.4	1343.3	**1822.0**	1969.9	1168.3	1307.0	2383.4
A/Heilongjiang-Xiangyang/1134/2011	3506.3	3480.2	5123.0	3514.3	356.0	976.7	1657.1	245.9	557.9	**7094.8**	2056.7	168.3	658.3
A/Perth/16/2009nib-64	4961.8	13872.0	8102.7	2771.2	630.3	3502.5	2644.5	1079.5	441.6	1663.8	**2458.4**	418.4	748.3
A/Tasmania/1018/2015	6503.6	7894.2	5204.6	1298.1	2335.3	2927.7	1349.1	6451.6	2374.2	709.1	2659.2	**1150.5**	977.3
A/Alaska/251/2015	7291.7	8216.5	7274.8	1247.6	1050.4	7445.9	1975.1	348.6	1070.2	1828.5	1142.7	2300.4	**3418.1**
A/Singapore/Infimh-16-0019/2016	2564.5	3869.9	3206.3	1119.2	1038.5	732.7	545.2	252.3	1308.7	196.5	328.1	399.6	778.4
A/Wisconsin/16/2015	6157.8	6249.7	3088.6	693.4	998.2	1259.1	383.6	73.1	595.7	362.7	415.4	442.8	723.5
A/Hong_Kong/3089/2017	713.6	1372.5	1290.5	391.8	312.4	670.9	231.0	144.6	161.5	143.3	88.2	317.5	702.9
A/Nagano/2153/2017	784.6	798.8	567.6	102.6	215.5	530.1	158.5	97.5	182.8	145.2	108.7	172.4	332.8
A/Sweden/3/2017	2250.6	1249.6	2688.6	1818.4	785.2	443.3	632.2	726.1	3344.3	553.2	512.0	910.7	2153.6
A/Moramanga/1907/2017	1126.6	1371.0	720.8	205.3	185.9	1073.8	339.2	212.5	335.6	228.0	201.0	396.1	603.7
A/Helsinki/823/2013	1130.4	1408.4	1382.9	491.8	77.1	1930.9	324.0	141.1	133.6	431.4	289.4	90.0	106.9
A/Helsinki/941/2013	391.1	379.7	662.2	345.4	19.2	837.0	227.2	32.7	25.7	72.6	111.1	23.7	58.9
A/Ohio/13/2017	396.6	554.6	500.2	247.4	56.6	377.9	185.1	112.0	75.2	168.4	219.8	80.1	10.0
A/Ohio/62/2012	445.7	644.5	694.0	157.0	33.1	1024.6	207.9	37.9	77.9	98.5	152.6	86.9	22.5
A/Ontario/Rv3236/2016	54.0	99.2	101.7	218.0	10.0	51.7	43.8	10.0	19.2	10.0	36.9	41.1	10.0
A/Indiana/08/2011	34.4	72.5	110.4	177.3	22.4	43.1	46.8	31.4	10.0	40.6	36.4	10.0	10.0
A/Minnesota/11/2010	59.4	146.7	91.6	17.5	16.4	44.0	39.0	10.0	10.0	41.1	30.8	10.0	10.0

669

670 **Table S3. NAI titers against H6N2 viruses of ferret sera obtained after the boost (Part II of II).**

Sera	Sin16	Wis15	HK17	Nag17	Swe17	Mor17	Hel823	Hel941	Ohi17	Ohi12	Ont16	Ind11	Min11
A/Switzerland/9715293/2013	1291.6	939.6	1097.8	210.5	514.9	460.1	160.2	706.4	422.8	1072.5	354.5	227.5	302.5
A/Hong_Kong/4801/2014	636.5	780.7	1312.1	30.8	178.6	231.7	55.5	229.9	221.4	143.0	122.2	93.4	307.2
A/Texas/50/2012	436.8	556.3	462.7	17.2	242.5	288.5	53.2	656.4	73.0	295.0	482.4	16.0	149.6
A/Victoria/361/2011(Ivr-165)	568.2	1881.1	1227.3	108.5	293.8	407.7	79.3	1203.0	290.1	561.0	793.8	125.4	393.1
A/Newcastle/67/2016	192.6	246.4	411.3	18.3	70.8	125.6	206.8	259.5	893.7	1553.0	1089.8	10.0	1619.5
A/Estonia/91621/2015	133.6	137.5	252.2	10.0	78.5	10.0	112.6	76.3	96.2	268.4	110.6	38.7	83.6
A/Utah/11/2011	212.4	753.0	215.9	41.4	138.5	265.5	100.4	549.1	208.9	1246.7	922.8	240.0	466.7
A/Gambia/G0071436/2012	390.8	532.3	694.8	37.3	174.6	139.2	296.9	470.4	233.7	154.4	423.5	157.8	709.3
A/Hanoi/Eli15597/2015	225.9	629.8	592.7	152.6	318.2	174.4	216.5	209.5	615.2	207.1	556.5	1205.8	669.2
A/Heilongjiang-Xiangyang/1134/2011	79.9	257.3	65.1	10.0	77.1	34.9	475.2	76.0	236.7	1330.2	70.6	48.1	127.2
A/Perth/16/2009nib-64	263.1	535.5	249.8	10.0	102.5	103.7	552.5	519.6	250.2	418.2	81.2	113.6	161.1
A/Tasmania/1018/2015	714.6	342.3	1149.8	178.8	321.5	551.2	363.1	1440.4	407.4	2702.2	819.1	463.8	689.9
A/Alaska/251/2015	655.6	1029.8	579.3	451.3	764.5	396.5	111.7	468.9	16.5	72.8	88.1	10.0	22.4
A/Singapore/Infimh-16-0019/2016	**3746.2**	1772.7	7210.9	1390.6	1637.5	1258.2	151.7	2123.3	94.6	282.6	68.0	10.0	122.3
A/Wisconsin/16/2015	772.0	**5850.3**	678.1	373.4	680.7	420.1	10.0	134.2	15.8	74.7	10.0	10.0	10.0
A/Hong_Kong/3089/2017	1534.5	708.7	**4119.2**	762.8	2114.3	744.7	297.3	324.9	10.0	10.0	10.0	10.0	10.0
A/Nagano/2153/2017	501.4	157.0	1131.7	**960.8**	258.6	313.2	94.3	115.9	85.6	136.8	10.0	10.0	54.6
A/Sweden/3/2017	5336.2	1167.5	7099.8	1132.6	**8452.0**	4595.1	506.4	2310.2	133.0	199.5	323.9	27.2	58.5
A/Moramanga/1907/2017	1060.6	273.0	3033.6	258.9	1286.0	**6330.8**	75.6	143.2	57.3	106.0	96.7	10.0	70.4
A/Helsinki/823/2013	519.3	215.9	745.1	10.0	326.8	113.1	**5933.4**	11949.0	33.1	87.9	85.5	32.4	46.8
A/Helsinki/941/2013	257.3	79.5	156.3	10.0	153.0	10.0	3729.4	**17816.2**	17.3	64.1	10.0	10.0	10.0
A/Ohio/13/2017	28.9	10.0	10.0	10.0	10.0	10.0	221.2	137.9	**2567.9**	28683.0	4819.3	781.1	4943.5
A/Ohio/62/2012	10.0	10.0	10.0	10.0	10.0	10.0	77.1	70.1	5592.0	**3811.0**	397.1	281.1	921.4
A/Ontario/Rv3236/2016	10.0	10.0	10.0	10.0	10.0	10.0	22.4	21.3	194.8	1500.5	**6167.6**	159.3	846.2
A/Indiana/08/2011	10.0	10.0	10.0	10.0	10.0	10.0	17.4	16.0	146.4	3741.8	486.8	**2910.9**	2498.3
A/Minnesota/11/2010	10.0	10.0	10.0	10.0	10.0	10.0	55.0	17.3	202.3	509.1	726.6	380.2	**4375.6**

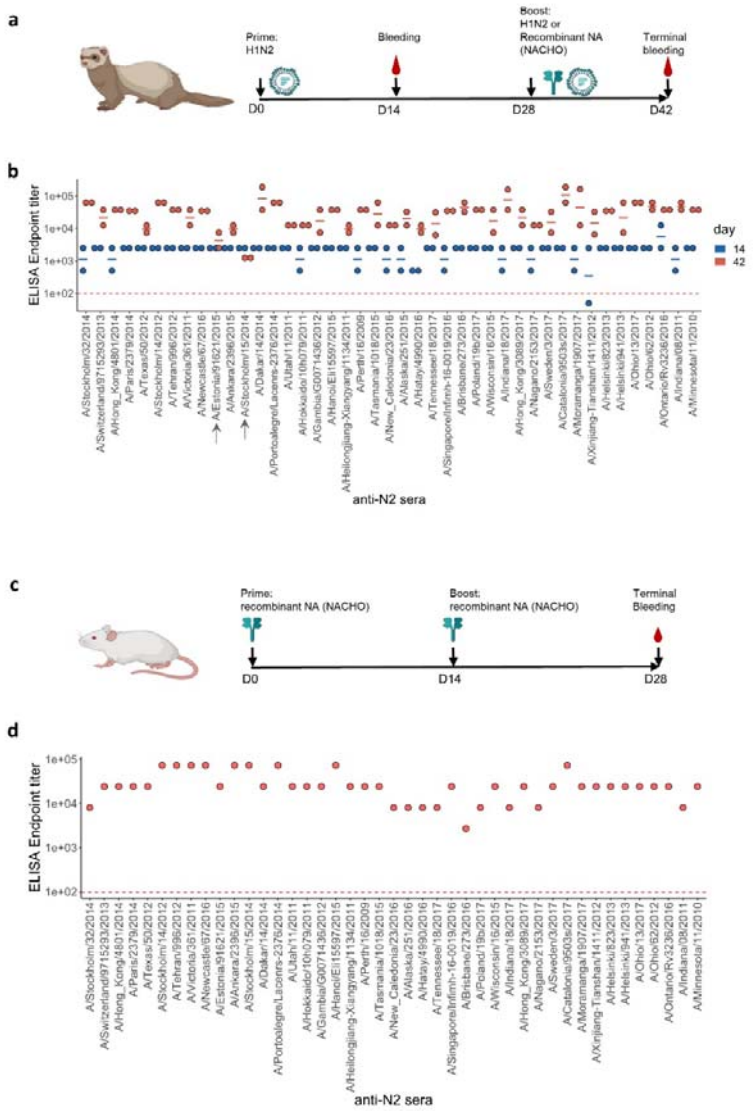

Figure 1. Generation of anti-N2 sera panel from ferrets and mice. (a) Ferret immunization and blood sampling scheme. The second immunization on day 28 was performed with homologous NACHO except for the ferrets that had been primed with $H1N2_{A/Estonia/91621/2015}$ or $H1N2_{A/Stockholm/15/2014}$, which were infected again on day 28 post prime with the same H1N2 viruses. (b) Homologous NACHO ELISA titer of ferret sera sampled on day 14 days after inoculation with H1N2 virus and 2 weeks after the boost with recombinant NA or by re-inoculation with $H1N2_{A/Estonia/91621/2015}$ or $H1N2_{A/Stockholm/15/2014}$ (indicated by arrows on the X-axis). (c) BALB/c immunization and blood sampling scheme. (d) Homologous NACHO serum IgG titers in pooled sera from mice that were immunized twice with recombinant NA. Mouse and ferrets representation were created with BioRender.com (2023).

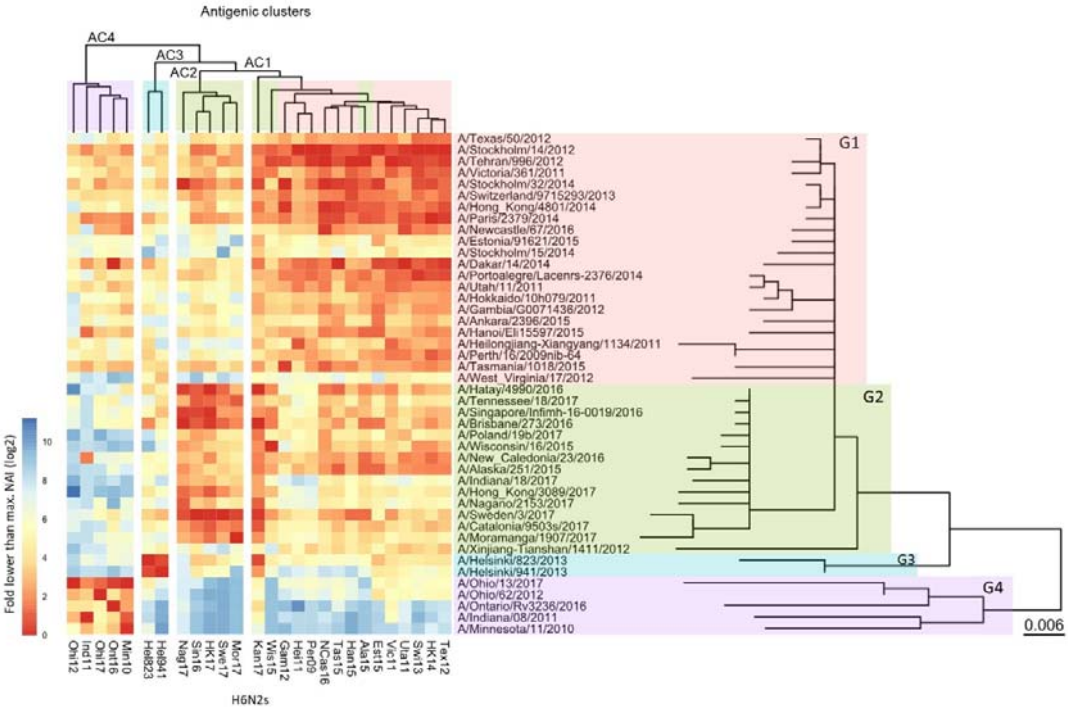

Figure 2. Breadth of N2 NA inhibition. Phylogenetic tree based on the N2 NA head domain amino acid sequences and heat-map representing the average of normalized neuraminidase inhibition per H6N2 [$\log_2$ (max NAI/NAI)] determined in ferret sera after the boost (listed vertically). The red-to-blue scale indicates high-to-low NAI observed in ELLA against the H6N2 reassortants (listed at the bottom). UPGMA clustering of H6N2s inhibition profiles are shown on top of the heat map and coloured according to the phylogenetic groups.

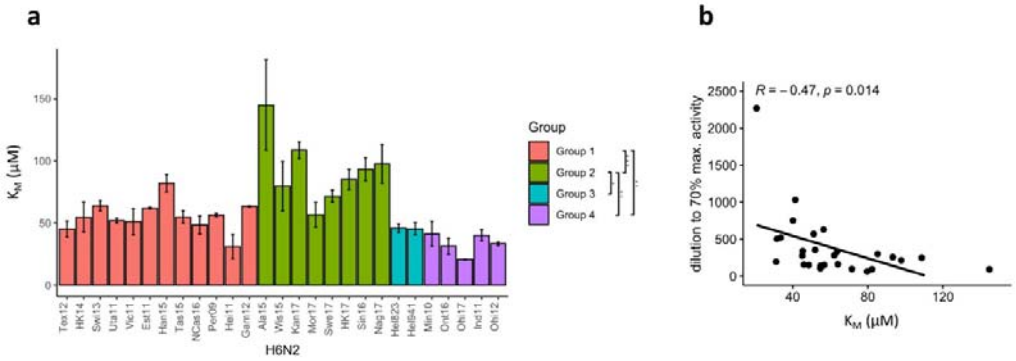

690
691 **Figure 2. Figure supplement 1. The N2 NA substrate affinity is distinct in the N2 phylogenetic**
692 **groups**. (a) K_M was determined for each H6N2 reassortant virus using the fluorogenic substrate
693 MUNANA. N2 NAs are coloured according to the phylogenetic groups. Global test comparing the 4
694 groups was done using ANOVA (P= 2.4e-05) and pairwise comparison performed using Wilcoxon,
695 ***P< 0.001, **P< 0.01, *P< 0.05. (b) Scatter-plot and correlation between the K_M values and
696 dilutions required to obtain 70% max activity in ELLA.

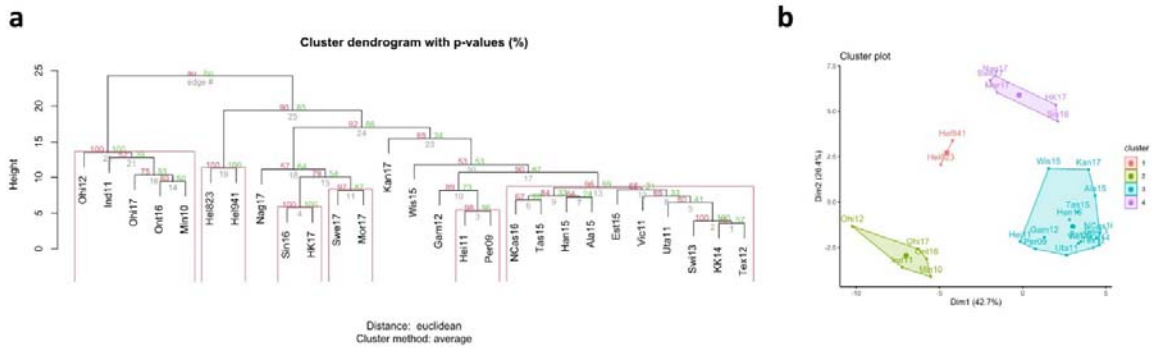

697

698 **Figure 2. Figure supplement 2. Antigenic relationship between NA of the H6N2 viruses.** (a)
699 Hierarchical clustering based on multisampling and multiscale bootstrap resampling. Approximately
700 unbiased p-values (AU) are shown in red, bootstrap values in green, and edge values in grey. The red
701 brackets represent the clusters with AU > 95%. (b) K-means clustering represented using principal
702 component analysis (k=4).

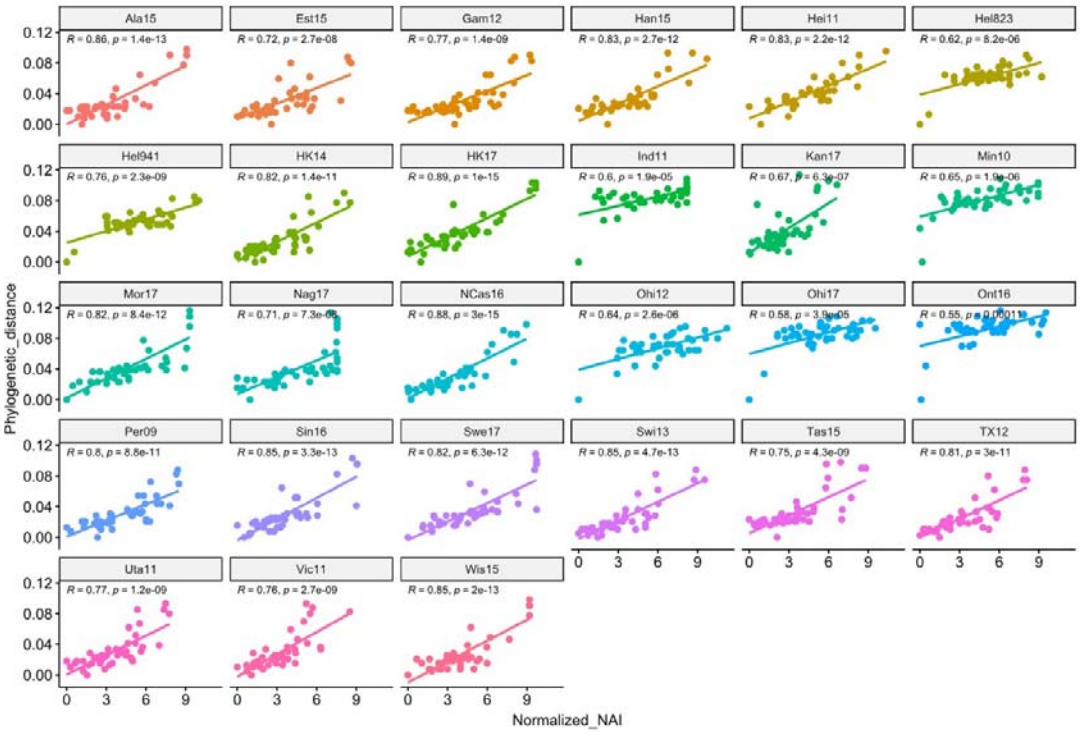

Figure 2. Figure supplement 3. Correlation of NAI fold reduction and phylogenetic relatedness. Scatter plot shows the phylogenetic distances (y-axis) and Normalized NAI as fold reduction relative to the maximal inhibition [$\log_2$ (max NAI/NAI)] (x-axis). Each graph represents one of the 27 H6N2s that were tested.

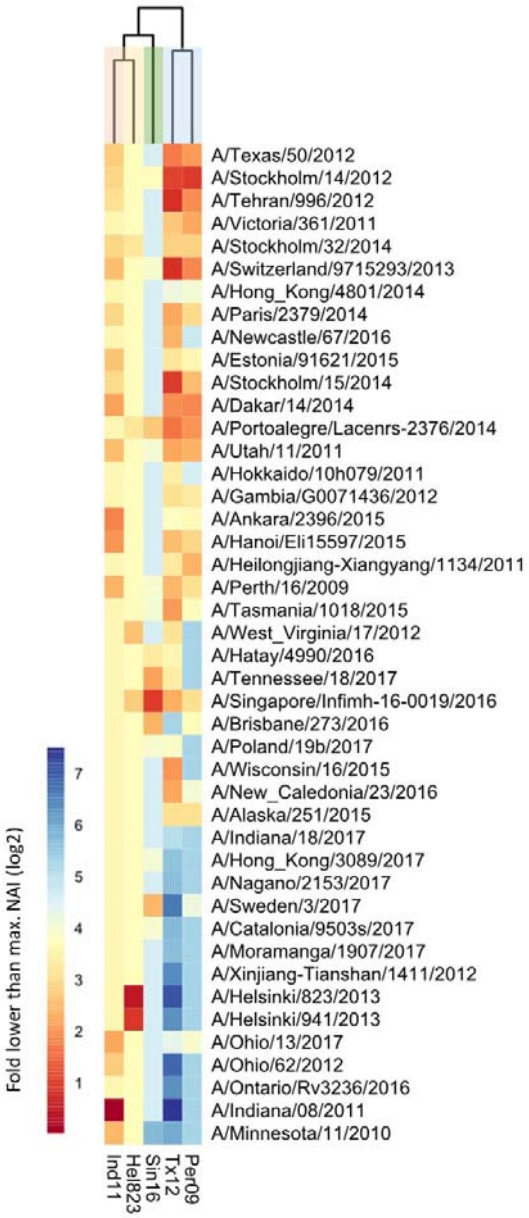

Figure 2. Figure supplement 4. Breadth of N2 inhibition of sera from ferrets primed by H1N2 infection only. Heat-map representing the average of normalized neuraminidase inhibition per H6N2 [$\log_2$ (max NAI/NAI)] determined in ferret sera 2 weeks after infection. The red-to-blue scale indicates the fold reduction compared to the max NAI observed in ELLA against the H6N2 reassortants (listed at the bottom). UPGMA clustering of H6N2 inhibition profiles are shown on top of the heat map and coloured according to the phylogenetic groups.

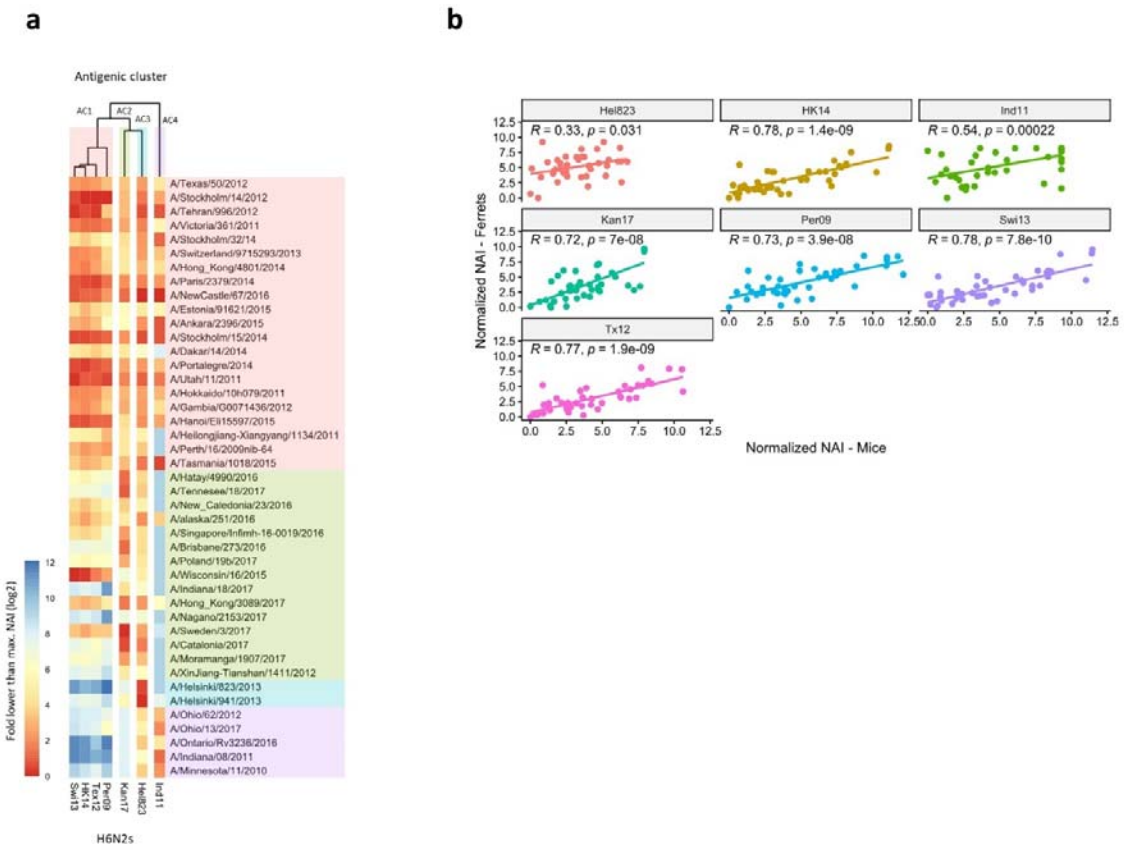

715

716 **Figure 2. Figure supplement 5. Breadth of N2 inhibition is confirmed in mouse sera.** Heat-map
717 representing the average of normalized neuraminidase inhibition per H6N2 [$\log_2$ (max NAI/NAI)]
718 determined in mice sera after the boost (listed on the right). The red-to-blue scale indicates low-to-
719 high NAI observed in ELLA against the H6N2 reassortants (listed at the bottom). UPGMA clustering of
720 H6N2 inhibition profiles are shown on top of the heat map and coloured according to the
721 phylogenetic groups. (b) **Correlation of NAI between mice and ferrets**. Scatter plot shows the
722 normalized NAI as fold reduction from maximal inhibition [$\log_2$ (max NAI/NAI)] from ferrets (y-axis)
723 versus mice (x-axis). The 7 H6N2s tested are indicated in graph titers.

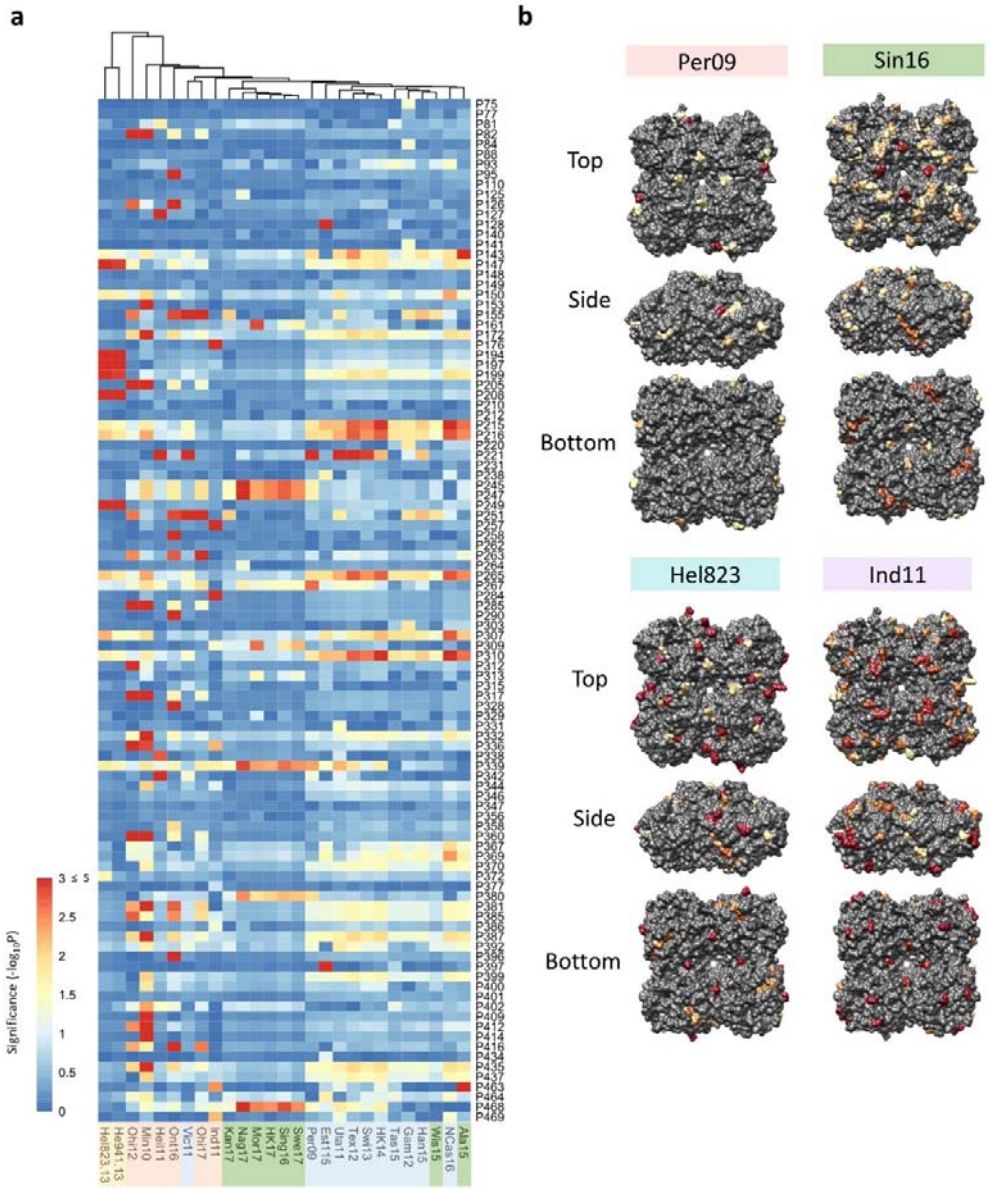

Figure 3. Association analysis reveals impact of amino acid mutations on NAI. (a) Association study performed for each H6N2 virus (listed at the bottom) to determine the probability of each variable amino acid (listed on the right) present in the panel of 44 NAs to impact the NAI. The red-to-blue scale represents significance values ($S=-\log_{10}P$) associated with each amino acid substitution. The dark red in the color scale represent all values that are equal or higher than 3 (corresponding to p-values ≤ 0.001). The colour shades on the bottom side indicate the distinct phylogenetic groups. (b) The significant values ($p<0.05$) were represented in the surface of N2 tetramer (PDB accession number 4H53) for one representative strain of each phylogenetic group with a yellow to red scale of significance ($-\log_{10}P$).

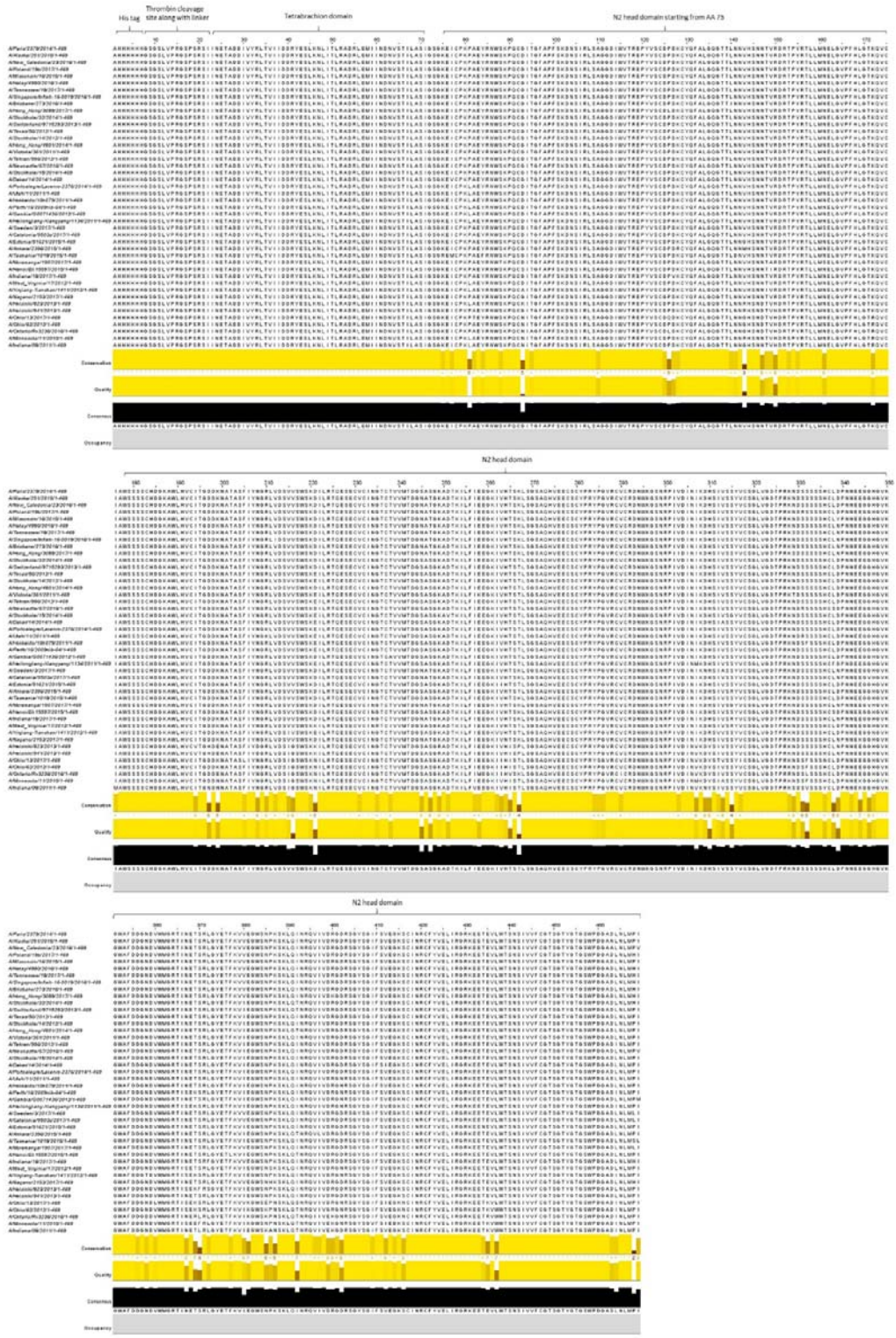

Figure 3 – figure supplement 1. Protein sequence alignment of N2 NACHO panel used for immunization. The sequence of recombinant NA that was used for boosting ferrets or to prime/boost BALB/c mice was aligned starting from the HIS-tag, tetrabrachion and followed by NA head domain, as depicted on top of the sequences.

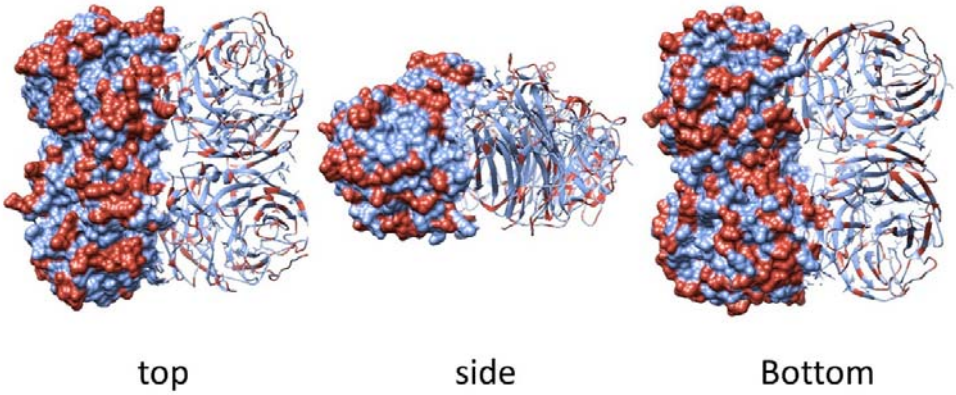

739

740 **Figure 3 – figure supplement 2. Geometrical distribution of amino acid substitutions in the N2**
741 **structure.** The surface and ribbon representation indicate the geometrical distribution of the amino
742 acid substitutions that are present in the panel of 44 N2 NAs used as immunogens in the study.
743 Substitutions are highlighted in red on the model structure of N2 from H2N2 (A/RI/5+/1957, PBD
744 4H53).

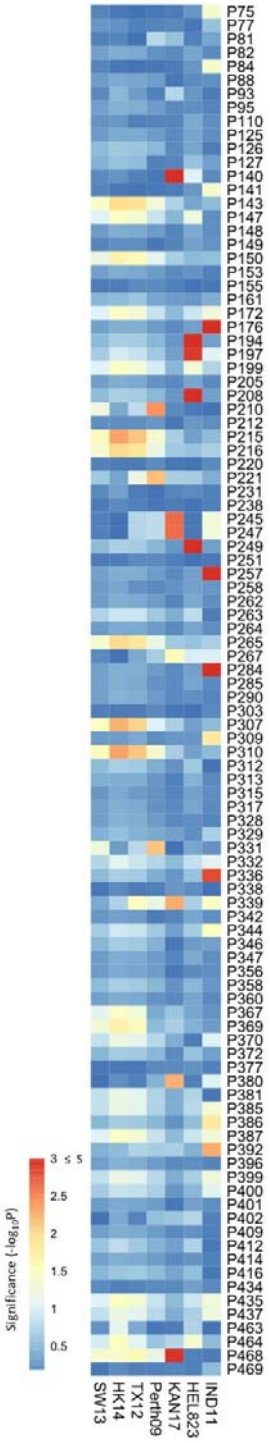

745

746 **Figure 3 – figure supplement 3. Association study was performed on data obtained from mouse**
747 **sera.** (a) Association study performed for each H6N2 virus (listed at the bottom) to determine the
748 probability of each variable amino acid (listed on the right) present in the panel of 44 NAs to impact
749 NAI. The red-to-blue scale represents significance values ($-\log_{10}P$) associated with each variable
750 amino acid.

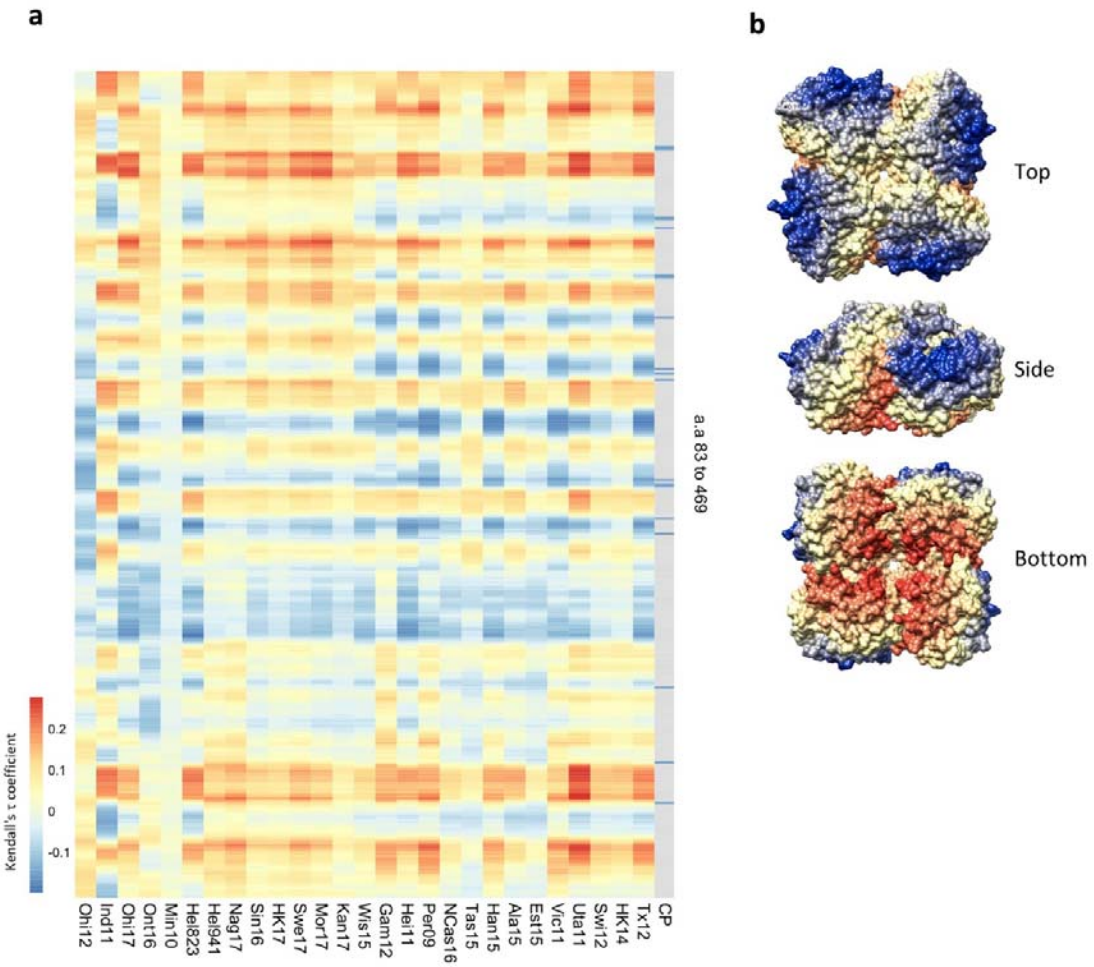

751

752 **Figure 4. Residues close to the catalytic pocket are more likely to impact NAI.** (a) Significance
753 values (102 variable amino acids) obtained from the association study were correlated to the
754 distance between every amino acid and each of the variable amino acids in the NA structure. The
755 red-to-blue scale represents the Tau values obtained in the Kendall correlation. Amino acids 83 to
756 469 are shown from top to bottom in the heatmap. The H6N2s used in the NAI panel are listed at the
757 bottom. The grey column (catalytic pocket (CP)) indicates the residues that are part of the catalytic
758 pocket that directly interact with substrate (R118, D151, R152, R224, E276, R292, R371, and Y406)
759 and the residues that play a key role in stabilizing the catalytic site (E119, R156, W178, S179, D198,
760 I222, E227, H274, E277, N294, and E425). (b) Tau values obtained from Tex12 H6N2 correlation are
761 represented on the surface of the N2 structure of A/RI/5+/1957 (PBD 4H53).

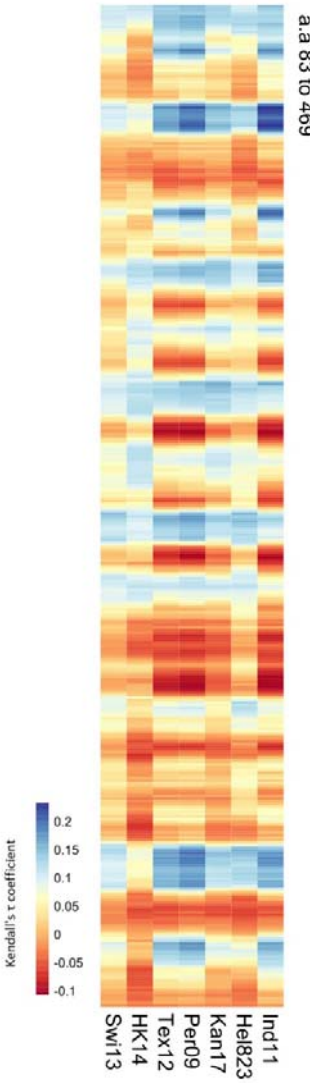

Figure 4 – figure supplement 1. Correlation of values obtained from the mouse sera panel and amino acid distances. (a) Significance values (102 variable amino acids) obtained from the association study were correlated to the distance between every amino acid and each of the variable amino acids in the NA structure. The red-to-blue scale represents the Tau values obtained in the Kendall correlation. Amino acids 83 to 469 are shown from top to bottom of the heatmap. The H6N2s used in the NAI panel are listed at the bottom.

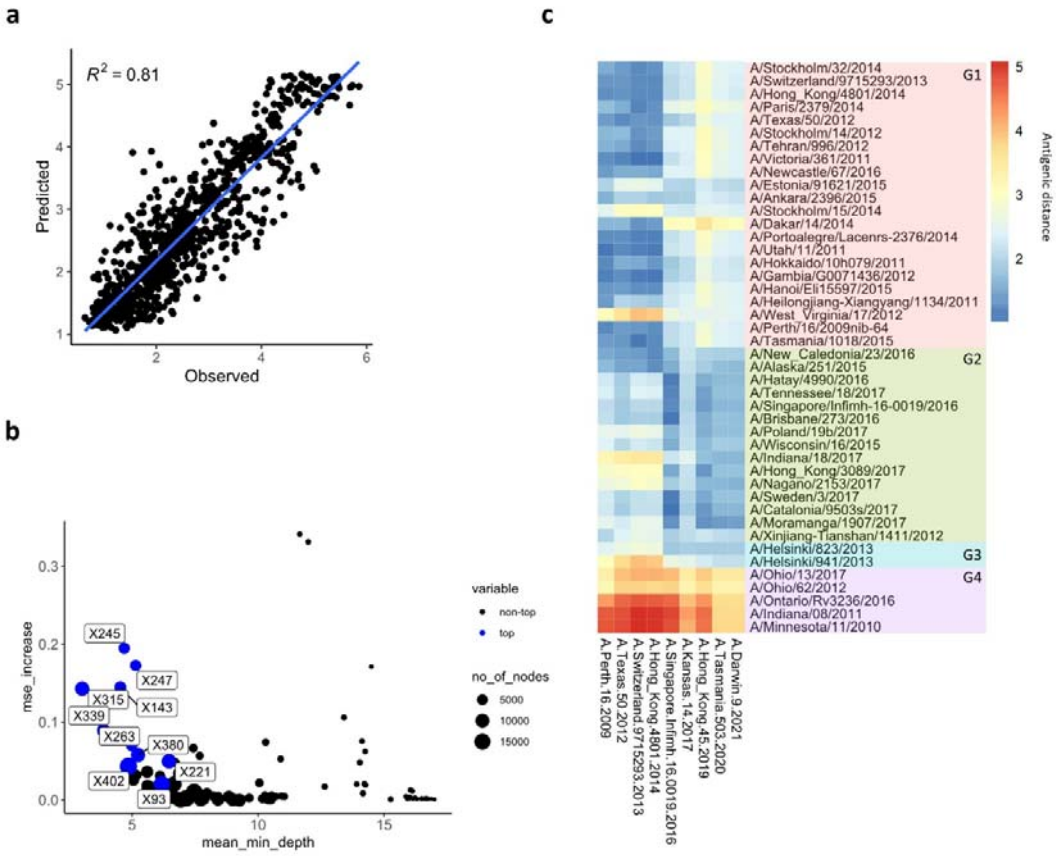

Figure 5. Prediction of N2 antigenicity based on machine learning. (a) Predicted *vs* observed normalized NAIs are shown. (b) Multi-way importance plot indicating the increase in mean standard error, the mean depth, and number of nodes. The top 10 most important amino acid changes are highlighted in blue and annotated with their position in the NA sequence. (c) The heatmap indicates the predicted antigenic distances of N2s from recent H3N2 isolates (at the bottom of the heatmap) relative to the N2s that were used in the NAI breadth panel (listed vertically). The antigenic distances were calculated based on NA protein sequence.

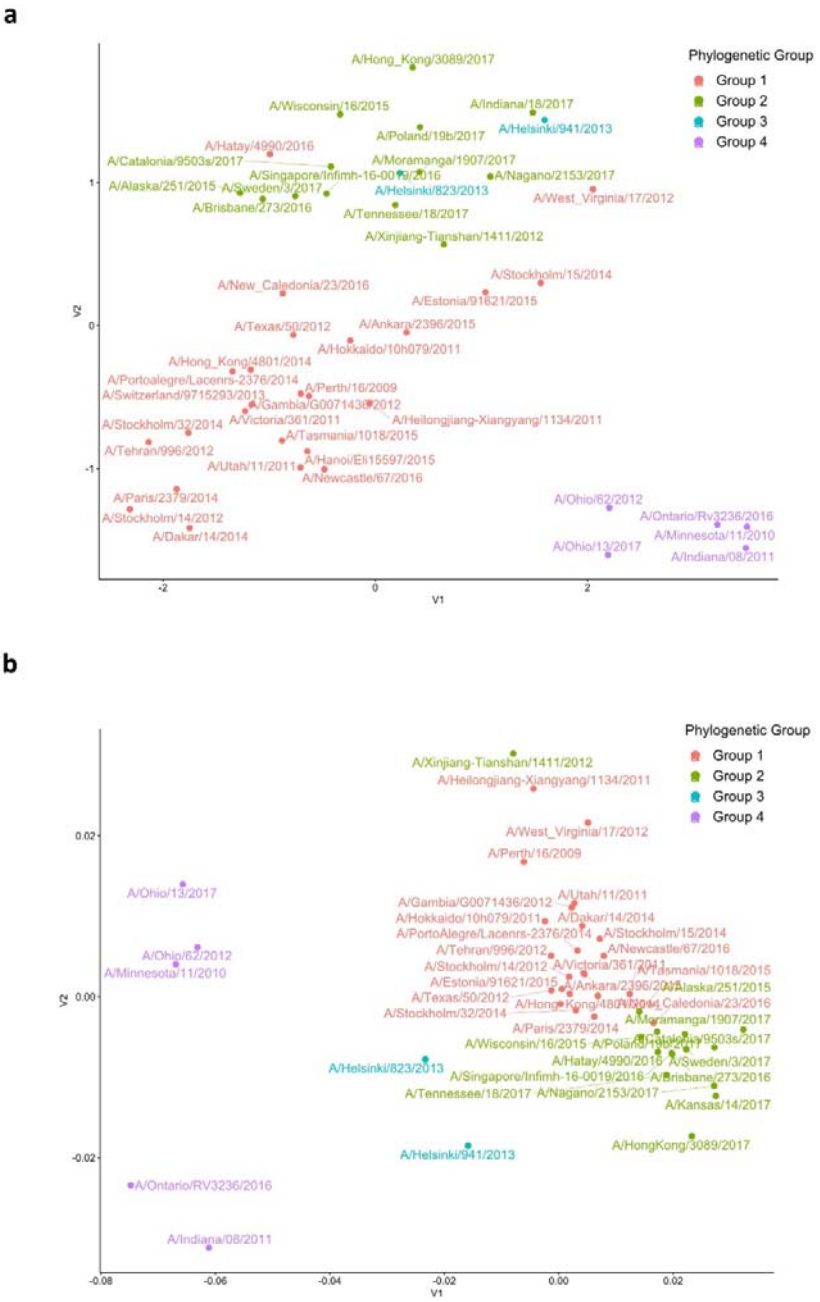

Figure 5 – figure supplement 1. **Multidimensional scaling defining antigenic and phylogenetic cartography of N2s.** (a) Average antigenic distances were plotted using classical MDS, N2 groups are colored according to the phylogenetic groups. (b) Pairwise comparison of amino acid sequences of the NA head domain was used to generate a matrix of phylogenetic differences that is represented using classical MDS. N2s are colored according to the phylogenetic groups.